Accepted Manuscript

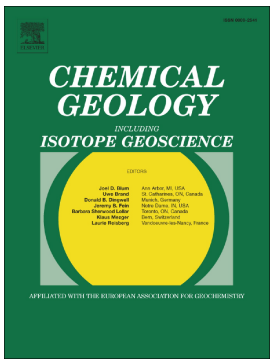

Belingwe komatiites (2.7Ga) originate from a plume with moderate water content, as inferred from inclusions in olivine

E.V. Asafov, A.V. Sobolev, A.A. Gurenko, N.T. Arndt, V.G. Batanova, M.V. Portnyagin, D. Garbe-Schonberg, S.P. Krasheninnikov

PII:	S0009-2541(17)30623-X
DOI:	doi:10.1016/j.chemgeo.2017.11.002
Reference:	CHEMGE 18530
To appear in:	*Chemical Geology*
Received date:	6 June 2017
Revised date:	27 October 2017
Accepted date:	3 November 2017

Please cite this article as: E.V. Asafov, A.V. Sobolev, A.A. Gurenko, N.T. Arndt, V.G. Batanova, M.V. Portnyagin, D. Garbe-Schonberg, S.P. Krasheninnikov , Belingwe komatiites (2.7Ga) originate from a plume with moderate water content, as inferred from inclusions in olivine. The address for the corresponding author was captured as affiliation for all authors. Please check if appropriate. Chemge(2017), doi:10.1016/j.chemgeo.2017.11.002

Belingwe komatiites (2.7 Ga) originate from a plume with moderate water content, as inferred from inclusions in olivine.

Asafov E.V[1]., Sobolev A.V.[1,2], Gurenko A.A.[3], Arndt N.T.[2], Batanova V.G.[1,2], Portnyagin M.V.[1,4], Garbe-Schonberg D.[5], Krasheninnikov S.P.[1]

1. Vernadsky Institute of Geochemistry and Analytical Chemistry, Russian Academy of Sciences, 19 ul. Kosygina, Moscow 119991, Russia.
2. ISTerre, Univ. Grenoble Alpes, CNRS, IRD, IFSTTAR, 38000 Grenoble, France.
3. Centre de Recherches Pétrographiques et Géochimiques (CRPG), UMR 7358, Université de Lorraine, 54501 Vandoeuvre-lès-Nancy, France.
4. GEOMAR Helmholtz Centre for Ocean Research Kiel, Wischhofstrasse 1-3, 24148 Kiel, Germany.
5. CAU Kiel University, Institute of Geosciences, Ludewig-Meyn-Strasse 10, 24118 Kiel, Germany.

Keywords: Belingwe Greenstone Belt; Archean Zimbabwe Craton; olivine; spinel; melt inclusions; water; carbon dioxide; chlorine; mantle; temperature; oxygen fugacity; SIMS; EPMA; LA-ICP-MS; komatiite

Corresponding author: Mr. Evgeny Vladimirovich Asafov, M.D.

Corresponding Author's Institution: Vernadsky Institute of Geochemistry and Analytical Chemistry, Russian Academy of Sciences, 19 ul. Kosygina,Moscow 119991, Russia.

Abstract

Major and trace elements, and volatile components have been measured in melt inclusions in olivine from fresh 2.7 Ga old komatiites from the Reliance Formation of the Belingwe Greenstone Belt, Zimbabwe. Reconstructed compositions of melt inclusions contain 20-23.5 wt.% MgO and up to 0.3 wt.% H_2O; these compositions probably represent those of the erupted lava. In inclusions in relatively evolved (low Fo) olivines, an excess of Na_2O, CaO, Li, La, Cu, Rb, Y, Sc as well as volatile components (H_2O, F, Cl and S) relative to other highly incompatible elements is attributed to assimilation of seawater altered mafic material. No assimilation signature is observed for the most primitive melt inclusions hosted in the magnesium rich olivines. The primary melt composition, estimated using melt inclusions in the most magnesian olivine (Fo93.5), contains up to 27.5 wt.% MgO and ca. 0.2 wt.% H_2O. The presence of H_2O slightly depressed the liquidus temperature to ca. 1513°C. Our results suggest formation of the Belingwe komatiite magma at ca. 7 GPa pressure and ca. 1790 ^oC temperature in a mantle plume. The plume picked up water and probably chlorine through interaction with a hydrous transition mantle zone in the way similar to that previously proposed by Sobolev et al. (2016) for komatiites in Canada.

1. Introduction

Komatiites are the most MgO-rich and hottest volcanic rocks on Earth. Their anhydrous liquidus temperatures are estimated to be about 1600^{o}C, but their eruption temperatures and the mode of origin are uncertain because the amount of volatiles initially dissolved in komatiite magmas is poorly constrained (Arndt et al., 1998; Parman et al., 2004; Sobolev et al., 2016). The water contents in komatiite magmas have been debated since Viljoen and Viljoen (1969) first described komatiites. Most researchers now agree that komatiites result from melting in essentially dry and exceptionally hot mantle plumes (Arndt et al., 1998; Campbell et al., 1989; Connolly et al., 2011), and the alternative point of view – that komatiites are hydrous magmas that formed in subduction settings (Brooks and Hart, 1974; Allègre, 1982; Grove et al., 1997; Parman et al., 2004) – is now not widely accepted (e.g. Arndt et al. 2008; Berry et al., 2008).

Several attempts have been made to determine the concentration of water in komatiites. Parman et al. (2004) employed the compositions of pyroxenes to infer an extremely wet komatiite magma that originated in a supra-subduction setting, but most recent studies found far lower water contents. For example, Danyushevsky et al. (2002) estimated 0.2-0.3 wt.% of H_2O in the melt inclusions in olivine from Belingwe Greenstone Belt komatiites. Berry et al. (2008) measured low (0.10±0.02) Fe3+/∑Fe ratios in the melt inclusions using X-ray absorption near-edge structure, and used this to rule out oxidation and related diffusional H-loss from melt inclusions. Connolly et al. (2011) then used H_2O/Ce ratios to propose anhydrous and exceptionally high-temperature initial melts. On this basis, these authors proposed that the measured water contents are those of the original melt. However, the study by Shimizu et al. (2001) of melt inclusions in chrome spinel crystals from the Belingwe komatiites suggested the presence of up to 1.7 wt.% water in trapped melts and 0.8-0.9 wt.% H_2O in the primary komatiite magma. Finally, direct SIMS measurements of H_2O in melt inclusions in exceptionally magnesian olivine (up to Fo94.3 where Fo = Mg/(Mg+Fe) at%), independently supported by Sc-Y olivine-melt geothermometry, revealed up to 0.6 wt% H_2O in the primary melt of 2.7 Ga Abitibi komatiites (Sobolev et al., 2016).

Experimental approaches (Inoue and Sawamoto, 1992; Kawamoto et al., 1996) and combinations of experimental and petrological methods to study igneous minerals in komatiites (Allègre, 1982; Arndt et al., 1998; Arndt et al., 2008; Parman et al., 1997; Stiegler et al., 2012; Stone et al., 1997) have also been applied. Based on these studies, water contents in parental komatiite melts are now estimated to range from essentially zero up to 3wt.%.

Formation of komatiites in a hydrous mantle plume was originally proposed by Inoue (1994) and Hirose and Kawamoto (1995). Shimizu et al. (2001) supported the same model using

data from melt inclusions in chrome spinel and more recently, Sobolev et al. (2016) developed a similar idea using melt inclusions in olivine in Abitibi komatiites. The latter authors proposed that water was entrained into a mantle plume as it traversed the mantle transition zone deep in the Archean mantle. High Cl-concentrations (up to 0.2 wt%) measured in a series of melt inclusions implied a contribution from seawater. These Cl-enriched melt inclusions were found even in the most magnesium rich olivine (Fo94.1), suggesting that the contamination occurred at an early stage of magma fractionation, thereby precluding correct estimation of the initial water contents using the composition of late-stage igneous minerals such as pyroxene or amphibole, or H_2O contents of the evolved melt inclusions in spinel. Shimizu et al.'s, (2001) estimates of water content of Belingwe komatiites were extrapolated from the compositions of melt trapped in chrome spinel that crystallized from evolved magma and thus these water contents do not represent those of the primary melt.

Here we report new data for two representative samples of 2.7 Ga Ngezi Group komatiites from the Belingwe Greenstone Belt, Zimbabwe. Using an electron microprobe (EPMA), laser ablation inductively coupled plasma mass spectrometry (LA-ICP-MS) and an ion microprobe (SIMS), we obtained data on major and trace elements and volatile components (H_2O, F, Cl, S, CO_2) in the melt inclusions and in their host olivines. We also analyzed trace elements in the whole rocks, as well as the compositions of co-existing spinel and olivine in thin sections by ICP-MS and electron microprobe. The main goal of our study was to determine the pristine composition (i.e. unmodified by alteration, contamination and fractional crystallization) of the parental melts of these komatiites. We also estimate the volatile contents in the parental melts, discuss their chemical evolution (including the temperature and pressure of origin), and finally place new constraints on the deep mantle processes responsible for the origin of Archean komatiites.

2. Geological background

The Belingwe Greenstone Belt (Fig. 1) is located in the southern part of the Zimbabwe Craton, to the north of the Limpopo orogenic belt and directly east of the Great Dyke. This belt is a tight syncline, unconformably underlain by 3.5-3.6 Ga tonalitic crust, the Shabani Gneiss Complex (Bickle et al., 1975) and by greenstones of similar age (Bickle et al., 1977; Nisbet et al., 1977). The Belingwe Greenstone Belt comprises the Lower Greenstones (2.9 Ga Mtshingwe Group), which consists of three sedimentary formations whose deposition environment ranges from probable beach to deeper water conditions, and the unconformably overlying Upper Greenstones (2.7 Ga Ngezi Group). Dupré & Arndt (1990) reported a Pb-Pb age of 2692±9 Ma

for basalt within this unit. The Upper Greenstones comprise (from base to top) 300m of shallow-water sedimentary rocks of the Manjeri Formation, the predominantly basaltic and komatiitic 0.5-1-km-thick Reliance Formation, the 6-km-thick basaltic and andesitic Zeederbergs Formation, and the uppermost Cheshire Formation of shallow-water sedimentary rocks. There is strong evidence that the volcanic successions of the Reliance and Zeederbergs Formation erupted in shallow submarine conditions onto submerged continental crust (Bickle et al., 1975, Nisbet et al., 1977).

In this project we studied two olivine cumulates (samples Z4 and Z6) from the Reliance Formation. The samples were collected by N. Arndt in outcrops of Tony's flow, one of the best-exposed komatiite flows (Bickle et al., 1993). In addition we used new LA-ICP-MS data on the olivine phenocrysts from olivine cumulates MZ-4 from the same lava series studied previously by (Sobolev et al., 2007). By Archean standards, the samples are only moderately altered, as is reflected by their relatively low water content (ca. 3%), by totally serpentinized groundmass but partially preserved olivine phenocrysts, by the presence of serpentine and carbonate veins, and by oxygen, hydrogen and Rb-Sr isotopic systematics (Bickle et al., 1993). According to their Nd and Pb isotope compositions, the selected samples do not show evidence of continental crust contamination (Chauvel et al., 1993). Fresh chrome spinel and fresh relicts of olivine occur in the samples. Some of these contain crystallized melt inclusions, which we investigated in the course of this study.

3. Sample preparation

All sample preparation was performed at the Vernadsky Institute of Geochemistry and Analytical Chemistry Russian Academy of Sciences, Moscow, Russia. The hand specimens of Z6 and Z4 komatiites from the cumulate layers were crushed and several small pieces were used to prepare polished thin sections. Thin sections were then used for electron microprobe analysis of olivine, and of melt inclusions in olivine and spinel. Fragments with minimal signs of alteration were manually crushed in a steel mortar and ground to powder using an agate mortar. A portion of the powder was used for solution ICP-MS analysis and the remaining parts of the sample were separated into size fractions of <0.1 mm, 0.1-0.25 mm, 0.25-0.5 mm, from which fragments of fresh olivine containing melt inclusions were hand-picked under a binocular microscope.

Most melt inclusions were found to be concentrated near the grain cores. Melt inclusions typically have spherical or ellipsoidal shapes. They are up to 200 μm in diameter and comprise glass, a shrinkage bubble and tiny crystals of spinel, olivine and pyroxene (Fig. 2). In order to

homogenize the partially crystallized melt inclusions, the separated fresh and clean olivine grains were heated at 1250-1350°C for 5 minutes in a 1 atmosphere, high-temperature vertical furnace in a C-O-H atmosphere with buffered oxygen fugacity corresponding to the quartz-fayalite-magnetite buffer (QFM), then rapidly quenched to glass in water. The olivine grains were mounted in epoxy resin, then ground and polished to expose the glass inclusions. Quenched melt inclusions contained glass, spinel crystals and a shrinkage bubble. Inclusions larger than 20 μm were selected for chemical analysis. Smaller inclusions were ignored because their compositions could be affected by a boundary layer effect, which is expressed in elevated Al concentrations and inconsistent Si/Mg ratios.

Initially altered and/or cracked melt inclusions are easily recognized after heating because they have lost most of their volatiles due to direct connection with 1 atmosphere external pressure at high temperatures.

4. Methods

4.1. EPMA

Major element compositions of the melt inclusions and host olivines in the epoxy mounts, and the compositions of coexisting olivine-spinel pairs in thin sections, were measured by electron microprobe (EPMA). All samples were analyzed using the JEOL JXA 8230 at ISTerre, Grenoble, France. Operating conditions were 15 to 25 kV accelerating voltage and 900 nA probe current for olivine in thin sections and 300 nA probe current for separated olivine grains in epoxy mounts using protocol described in Batanova et al (2015). The accuracy of the data was controlled by measuring the reference San Carlos olivine during the analytical session (Batanova et al., 2015; Sobolev et al., 2007). For each olivine grain, two or more analyses were performed and the uncertainties were calculated as standard deviations. The melt inclusions were analyzed for the major elements, trace elements (titanium, potassium, manganese, chromium and phosphorus) and volatiles (chlorine and sulfur) at 15 kV voltage and 12 nA current using protocol described in Sobolev et al (2016). The analytical precision was assessed by including reference glasses GOR-132G (Jochum et al., 2006) and VG-2 (Jarosevich et al., 1980) measured as unknown in the analytical session. GOR-132G was used to monitor contents of major and trace elements and VG-2 for concentrations of Cl and S. The number of analyses performed for each inclusion ranged from 1 to 4, depending on the inclusion size. Uncertainties were estimated as standard deviations or, in the case if single analyses, the standard deviations for the reference material. Spinel was analyzed in thin sections at 20 kV voltage and 50nA current with a chromite standard as reference material (Batanova et al., 2011). The spinel crystals have skeletal habits

and only one measurement per grain was possible. Uncertainty was estimated as the standard deviation for reference chromite. ZAF corrections were used to eliminate matrix effects. Compositions of olivine are listed in Table 1, unprocessed EPMA data on the melt inclusions is listed in the Table A.2 (online supplementary material), data on the melt inclusions corrected for post entrapment crystallization (see Section 4.5 for details) and host olivines are given in the Table 2 and the compositions of spinel and coexisting spinel-olivine pairs are listed in Table A.1 and Table A.3 respectively (Online supplementary material).

4.2. SIMS

The CAMECA IMS 1280 HR2 and IMS 1270 E7 secondary ion mass spectrometers (SIMS) in CRPG, Nancy, France, were used to analyze CO_2, H_2O, Cl, S and F in the melt inclusions. A set of standards (ALV981-R23, ALV519-4-1, 30-2, 40-2, KL2-G, CY8406-02 and San Carlos olivine) was used to define calibration lines. The analytical details are provided in Sobolev et al. (2016).

4.3. LA-ICP-MS

We analyzed trace-element concentrations in melt inclusions and host olivine by LA-ICP-MS using an Agilent 7500s quadrupole mass-spectrometer coupled with a 193 nm Excimer laser ablation system GeoLas Pro (Coherent) at the Institute of Geosciences of the Christian-Albrecht University in Kiel, Germany. Laser spot size was 24-µm and 32-µm for inclusions and olivine, respectively. Ablation was performed with laser pulse frequency of 10 Hz and laser fluence of 10 J cm^{-2}. Olivine analyses were performed on three spots surrounding each inclusion, on areas pre-ablated for 3 s to reduce surface contamination. All analyses were performed in a large volume 'Zürich' ablation cell. Carrier gas was He (~1 L min^{-1}) with addition of H_2 (0.014 L min^{-1}), which were mixed with Ar (0.85 L min^{-1}) before introduction into spectrometer. Analyses were performed in time-resolved mode and included 20 s background measurement followed by 20 s sample ablation and signal measurement. Dwell time was 10 ms for all elements. Detailed description of the method is given in Sobolev et al. (2016). All trace element contents are listed in the Table 2.

4.4. Solution ICP-MS

Bulk rocks were analyzed by solution ICP-MS on a Thermo X series II at ISTerre, Grenoble, France following the (Chauvel et al., 2011) protocol. For analysis, 100 mg of rock powder were dissolved in Savillex beakers and Paar bombs in mixture of high purity HF and HNO_3. Final solution in 2% HNO_3 was diluted by factor of 5000. We used BR-24 as an external

standard and a set of internal standards (BHVO-2, BCR-2, Bir-1a, BEN and UBN). A five-element spike (Be, Ge, In, Tm, Bi) was added to the solution to correct for machine drift. Trace-element concentrations were calculated using methods published by Barrat et al. (1996) and Ionov et al. (2006). Operating conditions were: RF power 1400W, coolant gas 13L/min, Aux gas 0.8L/min, nebulizer gas 0.9L/min, pump speed 1mL/min, T°C cyclonic chamber = 2°C, Time uptake = 90s. Three runs were performed per analysis with the dwell time 10ms per element. The ICP-MS was washed out with an acid solution (HNO_3 5% + HNO_3 2% + HNO_3 2%) three times after every analysis

4.5. Data processing

Compositions of melt inclusions are listed in the Table A.2 (supplementary online material). Cracked inclusions that had lost volatiles during or before heating were identified by low Na, S and Cl concentrations and filtered out. As the compositions of the melt inclusions were affected by post entrapment crystallization of olivine on the walls of the melt inclusions and Fe-Mg diffusion between host olivine and included melt, we reconstructed the composition of originally trapped melts using the reverse Fe-Mg diffusion method (Sobolev and Danyushevsky, 1994). This method is based on the olivine-melt equilibrium model of (Ford et al., 1983) and uses the original FeO content of the melt. The latter was determined using the Fo content of the host olivine by modeling the crystallization of sample Z11 (Bickle et al., 1993), This sample was taken from chilled margin of komatiite flow and is thought to represent the quenched komatiite melt composition. The calculations were performed with the Petrolog3 software (Danyushevsky and Plechov, 2011).

Trace element and volatile element concentrations of the trapped melts were reconstructed using measured trace element contents in the melt inclusions normalized to the Al_2O_3 of the reconstructed melts in order to take into account the amount of the olivine, which crystallized on the walls of inclusions cavities.

Due to low solubility at low pressure, 40 to 90% of CO_2 can be lost to the bubbles in the inclusions (Esposito et al., 2011; Hartley et al., 2014; Mironov et al., 2015; Moore et al., 2015; Steele-Macinnis et al., 2011; Wallace et al., 2015). All studied melt inclusions do indeed contain a fluid bubble and therefore CO_2 concentrations measured in glasses represent only a small fraction of the CO_2 initially dissolved in the trapped melt. The measured water contents are also affected by this process but to lesser extent. To reconstruct the bulk CO_2 and H_2O contents in melts, we applied the method of Wallace et al. (2015) and used the VolatileCalc (Newman and Lowenstern, 2002) and Flincor (Brown, 1989) programs. Our calculations demonstrate that on average ~87% of the original CO_2 has been lost to the bubble. All measured CO_2 and water

contents were corrected using the described method. All reconstructed major, trace elements and volatile contents of the melt inclusions are listed in the Table 2.

4.6. Geothermometers and geobarometers

We used three geothermometers to estimate crystallization temperatures of the komatiite melt: a) partitioning of Sc and Y between olivine and melt (Mallmann and O'Neill, 2013), b) partitioning of Fe and Mg between olivine and melt (Ford et al., 1983), and c) partitioning of Al between olivine and spinel (Coogan et al., 2014). The temperatures calculated from Fe and Mg partitioning were then corrected for water dissolved in the melt using the equation of (Falloon and Danyushevsky, 2000).

To calculate Sc/Y temperatures, we used measured composition of olivines and the evaluated concentrations of Sc and Y in the komatiite melt as functions of MgO constrained using composition of bulk rocks following approach described in Sobolev et al. (2016):

Sc melt = 46.176-0.898*MgO

Y melt = 17.318-0.505*MgO

We used the published whole-rock data for Sc and Y (Bickle et al., 1993; Jochum et al., 1991; Nisbet et al., 1987) because Sc contents in melt inclusions appeared to have been strongly affected by diffusion like that of Fe (see Section 5.3 and 6.2). The Y contents in the melts calculated using the equation above are similar within error but overall are lower than those measured directly in inclusions by LA ICP-MS and then corrected for post entrapment crystallization.

The olivine-spinel thermometry was applied to olivine containing less than 91 mol% Fo, because only these co-exist with spinel (see Section 5.2 below). For the uncertainties on the temperature estimates, we used reported errors for these geothermometers: ±20 °C (2 standard errors) for Al-olivine-spinel geothermometer (Coogan et al., 2014) and ±24 °C (1 standard error) for Sc/Y olivine-melt geothermometer (Mallmann and O'Neil, 2013).

To estimate oxygen fugacity, we first used oxygen geobarometers based on the partitioning of V between olivine and melt (Mallman and O'Neil 2013). Measured V-concentrations in the melt inclusions could be affected by the redistribution between host olivine, daughter spinel and the melt (see Section 5.3 below) and therefore we estimated contend of V as a function of MgO using the whole rock data of (Puchtel et al., 2009) following method of Sobolev et al. (2016)

V melt = 297.18-5.8206*MgO.

This method gives a precision of 0.08 $\log_{10}fO_2$ units (one standard deviation, Mallmann and O'Neill, 2013). We also used compositions of the coexisting olivine-spinel pairs measured in the thin sections and the method of Ballhaus et al. (1991). The reported 1 standard error precision of this protocol is ±0.4 log units.

All uncertainties on our measurements are reported as 2 standard errors.

5. Results

5.1. Olivine

Representative compositions of olivine from Belingwe komatiites are listed in Table 1. These compositions are consistent with those reported by Renner et al. (1994) and Sobolev et al. (2007). The analyzed olivine cores are un-zoned and have Fo contents from 93.5 to 87.5 mol% (Fig. 3) while the rims show normal zoning to Fo85 (see Fig. 4 and Renner et al., 1994). Mapping of the trace-element distribution demonstrates that P, Cr and Al possess oscillatory zoning, typical for magmatic olivine (see Fig. 4 and Milman-Barris et al., 2008). On this basis, we conclude that the fresh olivine relicts were not affected by post-magmatic alteration or metamorphism and likely preserved their initial magmatic patterns.

5.2. Chrome Spinel

Chrome spinel occurs as late stage microcrystals in close contact with, but not included in, olivine. This phase started to crystallize when the olivine had the composition Fo90.9, as indicated by the kink in the trend in the Cr vs. Fo diagram (Fig 3). Compositions of spinel grains are given in Table A.1 (online supplementary material). Spinel crystals are un-zoned except for thin Fe-rich reaction rims composed of microcrystalline magnetite aggregates. However, spinel grains have a variety of compositions with Mg# [=Mg/(Mg+Fe^{2+})] ranging from 0.34 to 0.63 and [Cr# =Cr/(Cr+Al+Ti+Fe^{3+})] from 0.64 to 0.74. FeO/Fe_2O_3 ratios in spinel were calculated from stoichiometry. All studied spinel grains show no evidence of low-temperature re-equilibration with residual melt nor signatures of metamorphic alteration, excepting the magnetite rims (Barnes, 1998).

5.3. Melt Inclusions: major and trace elements

The studied melt inclusions are hosted in olivine Fo92.5-90.9 and their compositions are not significantly affected by spinel crystallization because olivine with this composition crystallizes alone. However, all heated melt inclusions contain small spinel crystals that crystallized after entrapment within the inclusions and were not melted completely, probably

because of insufficient experimental temperatures (1350°C or lower). Complete melting of the daughter spinel crystals would have increased the concentrations of Cr and V in the melts. Concentrations of these elements in melt inclusions should therefore be considered as minima.

The concentrations of major and trace elements in melt inclusions are listed in Table A.2 (uncorrected compositions, online supplementary material) and Table 2 (corrected for post-entrappment crystallization and volatile loss in the bubble) and plotted against MgO in Fig. 5 and Fig. 6. Reconstructed trapped melts have a relatively small range of compositions, from 19.8 to 23.6 wt.% MgO, which is much less than in the whole rock samples which cover a wide range of MgO contents from 15 wt.% in spinifex textured komatiites to ~45-50 wt.% MgO in olivine cumulates (Bickle et al., 1993, Nisbet et al., 1987, Puchtel et al., 2009).

Most of the measured immobile major and trace element contents in the melt inclusions are consistent with the data from whole rock samples and vary regularly as a function of MgO content. Differences in the Na, K, Ba, Rb and Pb contents of whole rocks and melt inclusions are related to the alteration that affected the Belingwe komatiites. The contents of these elements in bulk rocks are thus not representative for the original melt, whereas the melt inclusions preserved initial magmatic concentrations of these elements. Finally, a group of immobile trace elements (Sc, Y, V) correlate with MgO both in the melt inclusions and in the whole rock samples (Fig. 6) but there are small but systematic shifts between the melt inclusions and whole rock data.

The abundances of TiO_2, SiO_2, Al_2O_3, K_2O in the melt inclusions in more magnesian olivines plot on the tight trends that coincide with olivine control lines (Fig. 5). Na_2O and CaO also plot on tight trends, but these have steeper slopes than predicted by olivine fractionation. These elements display slight excess in the melt inclusions hosted by less magnesian olivine. The Al_2O_3/TiO_2 of the Belingwe komatiites yields an average of 21.3, a value close to the chondritic, which classifies them as Al-undepleted komatiites (Jahn et al., 1982; Nesbitt and Sun, 1976).

Trace element abundances in melt inclusions show larger scatter than the whole rock data (because of the larger analytical uncertainty of analyses of small inclusions) but they mostly plot close to the trends defined by the whole rock compositions (Fig. 6). Trace element concentrations of the melt inclusions, as well as previously reported whole rock data from the same flow, (Tony's Flow, Bickle et al., 1993) were normalized to 0.39 wt.% TiO_2 (average concentration in the studied melt inclusions) and to primitive mantle (Hofmann, 1988) to eliminate the effect of olivine crystallization or accumulation during or following eruption (Fig. 7). Averaged mantle-normalized trace-element patterns of melt inclusions are smooth but feature pronounced positive Sr anomalies, negative Pb anomalies and significant positive anomalies of volatiles (H_2O, F, Cl). Whole rock samples show similar REE patterns, positive Sr anomalies and significant positive Pb anomalies. In the whole rock samples, the mobile elements Pb, Rb, Ba and K do not preserve

initial features and have very wide ranges due to alteration, whereas in the melt inclusions they display tight areas without significant deviations. On this basis we conclude that the melt inclusions are minimally affected by post-entrapment alteration and preserve the original melt compositions.

The trace element patterns from melt inclusions display depletion in light rare earth elements (LREE; $(La/Sm)_n$=0.65±0.03) and flat heavy rare earth element (HREE) patterns ($[Gd/Yb]_n$=1.01±0.06). These values are characteristic of Al-undepleted (Group 1) komatiites described by (Jahn et al., 1982) and are consistent with previous studies of the Belingwe komatiites (Bickle et al., 1993; Puchtel et al., 2009; Shimizu et al., 2005).

5.4. Volatile contents in the melt inclusions

Representative analyses of volatiles in the melt inclusions, corrected for CO_2 loss and for post-entrapment crystallization (see Section 4.5), are listed in Table 2 and the uncorrected data in Table A.2 (online supplementary material). Measured CO_2 in glasses ranges from 3 to 43 ppm.

Water contents measured directly by SIMS in melt inclusions are subject to uncertainty due to a relatively high permeability of hydrogen in olivine, as demonstrated by numerous studies (Mei and Kohlstedt, 2000; Mironov et al., 2015; Portnyagin et al., 2008; Sobolev and Danyushevsky, 1994). Hence, prior to interpreting their original concentrations, it is important to determine whether the measured water contents were affected by diffusive loss or gain of H after entrapment. Measured water contents differ by 30-40% (averaged measured H_2O = 0.37 wt.% versus average corrected H_2O = 0.24 wt.%), from values corrected for post-entrapment crystallization and loss to the vapor bubble. The water contents show a significant negative correlation with the Fo content of host olivine (R^2=0.46 for 20 inclusions, confidence level 0.95) and hence with the MgO contents of the trapped melt. Plotted on Fig. 8 are correlation lines between the volatile contents in the melt inclusions hosted in Fo >91.5 and the Fo contents of the host olivines. Despite the low R^2, these melt inclusions are consistent within error with the olivine control line and hence are representative of the parental melt compositions. Of the major and trace elements that are incompatible with olivine (e.g. TiO_2, Na_2O, Rb, Li, Sc, V, Cu, Ce), most display positive correlations with the corrected water contents of the melt inclusions. There are also significant (on 95% confidence level) positive correlations between H_2O and S and F (Fig. 9). In contrast, no correlations are observed between the size of the melt inclusions and H_2O concentrations. All these observations suggest that water-concentrations in melt inclusions represent those of the originally trapped melts and do not show any significant loss or gain due to

diffusion through the host olivine, as also was demonstrated for the olivine hosted melt inclusions by Berry et al. (2008).

Questionable data on water contents was acquired from four data points in small (7-21μm) melt inclusions from the cumulate sample Z4. The average water content is 0.07 wt.% H_2O, markedly lower than 0.2-0.3 wt.% H_2O in sample Z6. The small size of the inclusions and the low water contents means that H_2O loss by diffusion cannot be excluded.

Corrected CO_2 and H_2O contents were used to estimate the equilibrium pressure using the VolatileCalc program. These calculations yielded an average pressure of 357 bars (Fig. 10) or 1.2 km depth. Our estimates likely represent the minimum pressure of magma fractionation due to partial degassing during magma ascent of CO_2 that was originally dissolved in the melt (Dixon et al., 1995). This is supported by relatively low CO_2/Ba (5-41.4) and CO_2/Nb (54.7-432.1) ratios compared to estimated ratios for the modern depleted mantle (CO_2/Ba=133±44, CO_2/Nb=505±168, Rosenthal et al., 2015). Thus, the data probably apply to the last vapor-melt equilibrium in the magmatic system. The calculated equilibrium fluid should have low H_2O/CO_2 mol ratios (less than 0.025). Hence, if the degassing of the melt occurred, the effect on H_2O contents was negligible because it should not exceed few % of total CO_2 loss.

Water, fluorine, chlorine and sulfur concentrations in the corrected trapped melts also show negative correlation with the forsterite content of the host olivine (Fig. 8). The melts trapped by the most MgO rich olivines closely follow olivine fractionation line, while those included in more evolved olivines tend to have more elevated volatile concentrations than predicted by olivine control alone.

Chlorine concentrations in the melts range from 269 to 595 ppm with an average of 407 ± 40 ppm. Two outliers are not included in the average. One of these is an extremely Cl-rich inclusion containing up to 1280 ppm and the other is a small melt inclusion (20 μm) with an unusually low Cl (84 ppm). The latter was excluded from further consideration. The major and trace element composition of the melt inclusion with extremely high Cl is similar to those in the other melt inclusions for both mobile and immobile elements (Fig. 5, Fig. 6).

Water, chlorine and fluorine contents of the trapped melts show significant excess when normalized to primitive mantle (Fig. 7).

5.5. Geothermometers

We applied two independent thermometers – Al in olivine-spinel and Sc/Y olivine-melt – to estimate melt temperatures and water contents (see Section 4.6). Estimated temperatures are listed in the Table 2.

The Sc/Y method was applied to olivines with Fo contents from 91 to 93.3 and to cases in which we know the compositions of the melts. (Fig. 11). The estimates demonstrate a wide scatter plotting from the dry liquidus down to the 2 wt.% H_2O liquidus line. The average estimated temperature for the most magnesian olivines (Fo 93.3-91.7, average Fo 92.2, N=20), based on Sc-Y thermometer, is 1448±21°C. This temperature is 31°C less than the dry liquidus temperature for the melt and thus provides evidence of a small but significant amount of water in the melt.

Al-in-olivine-spinel temperatures obtained for the more evolved olivines (88.7-90.9 mol.% Fo, listed in the Table A.3, online supplementary material) scatter between the dry and 0.5 wt.% H_2O liquidus lines (Fig. 11) and tend towards the dry liquidus line with decreasing Fo. The most primitive olivine-spinel pairs (Fo 90.2-90.9, average Fo 90.5, N=7) yield an average temperature of 1391±26°C, which is ~36°C lower than the average dry liquidus temperature for this range.

5.6. Oxygen fugacity in the komatiite magma

Oxygen fugacity in magmatic systems can be used to distinguish between magmas originating in different tectonic settings (Evans et al., 2012). Magmas in modern subduction settings tend to be more oxidized than magmas generated in modern plumes and mid-ocean ridges. The tectonic setting of komatiites is uncertain and the redox state of the komatiite magma may provide additional information on their origin and on the oxidation state of the Archean mantle. Our estimates of fO_2 are based on the Mallmann and O'Neil (2013) or Ballhaus et al. (1991) protocols (see Section 4.6), and the results are plotted in Fig. 11.

The oxygen fugacity for the most MgO rich olivines (Fo 91.7-93.3), calculated using the method of Mallmann and O'Neil (2013), implies relatively reduced conditions corresponding to QFM -0.3 to QFM -0.9 equilibria. ΔQFM values exhibit a negative correlation with olivine Fo and follow closed-system olivine crystallization conditions from ΔQFM-1.1 at Fo93.5. The method of Ballhaus et al. (1991) for olivine-spinel pairs gives results that follow closely the same line, within the reported errors.

6. Discussion

Even though the komatiites in the Belingwe belt are among the best-preserved Archean komatiites, they have undergone alteration and regional metamorphism that partially replaced igneous minerals with secondary hydrous minerals (Bickle et al., 1993). Although some of the

immobile major and trace elements (e.g., HFSE, REE, V, Sc, Y) preserve the initial melt characteristics, concentrations of mobile elements (Na, K, Ba, Rb, Pb) and volatiles were strongly affected by post-magmatic processes. Despite the alteration, Belingwe komatiites contain abundant relicts of fresh olivine. Melt inclusions hosted in these relicts have immobile major and trace element concentrations consistent with the whole rock data. They also preserved the concentrations of mobile trace elements and volatiles in the trapped melts. Moreover, melt inclusions in the most magnesian olivines follow olivine fractionation trends and thus can be used to reconstruct the initial melt composition and the original water contents.

6.1. Signs of contamination

Contents of SiO_2, Al_2O_3, TiO_2, K_2O and most of the trace elements in the trapped melts are consistent with olivine control lines for the entire compositional range of the host olivines (Fig. 4, 5). However, melt inclusions in the more evolved olivines display scatter about, but mainly above, the olivine fractionation line for the concentrations of Na_2O, CaO, Li, La, Cu, Rb, Y, Sc, as well as H_2O, Cl, F and S. This enrichment cannot result from the fractional crystallization of olivine but may be related to assimilation and fractional crystallization (AFC, except for Sc and Y – as discussed in a later section), which probably affected komatiites at a late stage of crystallization.

One possible source for the H_2O and Cl enrichment is seawater or high-salinity brines (Kent et al., 2002; Kent et al., 1999; Lassiter et al., 2002). As shown in Figure 12, two-component mixing of komatiite melt with seawater is inconsistent with the observed H_2O/Cl and K/Cl ratios in the melt, whereas mixing with high-salinity brine yields a range of compositions that coincides with the melt inclusion data as well as with data for altered MORB and OIB glasses (Kendrick et al, 2017). The contamination of komatiite melt could have taken place on its way to the surface via the assimilation of brine saturated sea-water altered oceanic crust (e.g. Lassiter et al, 2002). The relative excess of fluid-mobile elements in komatiite melt inclusions is not very large and is observed only for the most evolved melts, and it is therefore not possible to accurately model the contamination. Nonetheless, the compositions of the most primitive melt inclusions are consistent with the model of olivine fractionation and hence are representative of the parental melt.

6.2. Reconstruction of parental melt

To exclude the contamination effect from the calculations of the parental melt composition, we used a set of 7 inclusions that lacked pronounced contamination signatures in the most MgO rich olivines (Fo 92.1-92.5, Table 2). In our calculations, we assumed that the

initial melt was in equilibrium with Fo 93.5 – the most MgO-rich olivine analyzed in this and earlier studies (Bickle et al., 1993, Sobolev et al., 2007). To calculate the melt composition in equilibrium with this olivine, we used the reverse crystallization of olivine procedure in the Petrolog 3.0 software of Danyushevsky and Plechov (2011). To calculate the compositions of the melt in equilibrium with olivine we applied the models of Ford et al. (1983) and Herzberg and O'Hara (2002) and averaged the compositions of melts in equilibria with Fo 93.5 acquired using the two protocols. This makes sense, because as was shown recently by Krasheninnikov et al. (2017) testing of these models displays a certain temperature underestimation for the Ford et al. (1983) model and temperature overestimation for the Herzberg and O'Hara (2002) model for the temperatures exceeding 1450°C. The oxygen fugacity was based on V partitioning between the host olivine and melt (Mallmann and O'Neill, 2013), which corresponds to closed system crystallization starting at ΔQFM -1.1 (Fig. 11).

Our estimated primary komatiite melt contained 47±0.7 wt.% SiO_2, 27.5±2.9 wt.% MgO and 0.18±0.02 wt.% H_2O (Table 2). The calculated major element contents for the primary komatiite melt of the Belingwe komatiites are consistent with the 50-60% partial melting of peridotite KR4003 (Fig. 13), unlike the Abitibi komatiites which have too little SiO_2 (Herzberg, 2016; Herzberg and O'Hara, 2002; Walter, 1998). The pressure of melting is estimated to be ca. 7 GPa (Lee et al., 2009), and 60% partial melting of mantle peridotite at such depth would produce a residue composed of olivine with small amount of orthopyroxene, which is consistent with the proposed origin of Al-undepleted komatiite (Herzberg, 2004).

The systematic differences between the Sc and Y contents of melt inclusions and the whole rock data must be taken into account. Both elements are sensitive to temperature and may redistribute between the solid and liquid during cooling, and V, which has V^{3+} and V^{5+} forms, partitions differently between solid and liquid depending on the temperature and oxidation state of the magma. All studied melt inclusions come from cumulates, which are the lower parts of the flows and do not quench rapidly. We therefore suggest that the differences in the concentrations of Sc and Y between melt inclusions and whole rock samples results from redistribution of these elements between the trapped melts and host olivines. The V shift may be due to the presence of spinel crystals in the melt inclusions that were not completely resorbed during the experimental heating. As V is relatively compatible in spinel, these could reduce the V concentrations in the trapped melts. Thus, the whole-rock sample data may best represent the initial komatiite melt for these elements.

6.3. Independent approach for water contents

To check water contents measured directly in the melt inclusions by SIMS, we applied two independent geothermometers to estimate melt temperatures (see Section 4.6 for the uncertainties of the geothermometers) and evaluate the equilibrium water contents (see 5.5 Section). The estimated temperatures are listed in the Table 2.

Data obtained using the S/Y geothermometer may be influenced by Sc and Y redistribution between olivine and the residual melt during cooling (Fig. 11) and may therefore represent only the temperatures of the last olivine-melt equilibrium. But the temperatures obtained for the most MgO rich olivines (Fo 91.7 – 93.3) are likely to be unaffected by such re-equilibration and hence are more reliable. This is consistent with the fact that these olivines preserved their high Fo contents, suggesting that there was not enough time, or enough interstitial melt, to significantly change their compositions during later cooling. The estimated average temperature for the most magnesian olivines (average Fo 92.2, N=20), is 1450±22°C, which is 30°C lower than the dry liquidus temperature of melt in equilibrium with the olivine composition. The model of Falloon and Danyushevsky (2000) can be used to estimate the amount of H_2O that is needed to depress the temperature by 30°C. We calculate H_2O contents between 0.0-0.37 wt.% with a mean of 0.1±0.1 wt.% H_2O, which is consistent with the direct estimates using SIMS data (0.20±0.02 wt.%).

Even though the uncertainty of Sc/Y temperatures is large, this independent approach yields similar water contents, as obtained from direct SIMS measurements. This argues against the significant water gain or loss during the post-entrapment history.

Al-in-olivine-spinel temperatures scatter between the dry and 0.5 wt.% H_2O liquidus lines (Fig. 11) and trend towards the dry liquidus with decreasing Fo number. This variation is attributed to degassing of the melt in shallow crustal conditions. The most primitive olivine-spinel pairs (Fo 90.2-90.9, average Fo 90.5, N=7) yield an average temperature of 1391±26°C, which is ~36°C lower than the average dry liquidus temperature for this range. This difference corresponds to 0-0.5 wt.% H_2O (mean 0.13 wt.) in the melt and again is consistent within error with the direct SIMS measurements. However, these concentrations are significantly lower than those obtained by direct measurements of water in melt inclusions in spinel by Shimizu et al. (2001). We suspect that these melt inclusions were contaminated and do not accurately record the initial volatile contents of the magma. In contrast, our estimates on water obtained by direct measurements are consistent with the data reported by (Danyushevsky et al., 2002) and represent the maximum possible value.

6.4. Excess of H_2O and Cl in the parental komatiite melt

Our estimates of volatile contents in the parental melt are based on measurements of inclusions trapped in the most Mg-rich olivines. The concentrations of volatiles (H_2O, F, Cl and S) in these inclusions correlate with both the MgO of the melt and the Fo content of the host olivines and closely follow closed-system olivine fractionation paths (Fig. 8). We estimate 0.2 wt.% H_2O, 290 ppm Cl, 192 ppm S and 32 ppm F in the melt in equilibrium with Fo93.5.

Multiple correlations between water contents and concentrations of other volatiles, incompatible trace elements in melt inclusions and the forsterite content of the host olivine argue against H loss through diffusion. In addition, the estimated very low H_2O/CO_2 ratio of the equilibrium fluid ($[H_2O/CO_2]$ = 0.025; see Section 5.4) precludes significant degassing of H_2O before entrapment of melt inclusions, because the effect of degassing on H_2O contents was negligible as it should not exceed few % of the total CO_2 loss. All these suggest that the estimated H_2O contents, as well as concentrations of F, Cl and S in the parental melt, are reliable. However, the estimated concentrations of H_2O and Cl in Belingwe komatiites are much higher (H_2O/Ce>1100, Cl/K~1.3) than those estimated for modern mantle melts (H_2O/Ce=166, Cl/K=0.1) (Hofmann, 1988; Kendrick et al., 2017) (Fig. 14). On the other hand, recent experimental studies of high-pressure olivine polymorphs (wadsleyite and ringwoodite) have demonstrated that at the conditions corresponding to the mantle transition zone (14-22GPa, 1100-1400 °C), these phases are capable of holding significant amounts of Cl, F and H_2O (Roberge et al., 2015; Roberge et al., 2017).

6.5. Implications for the source of excess of water and chlorine

One possible source of excessive volatiles is H_2O-rich rock such as serpentinite, which could have been assimilated by the komatiite melt. In the results section, we noted that inclusions trapped in evolved olivine grains contain amounts of H_2O, F, S, Ca, Na in excess over those expected from closed-system olivine fractionation. This implies minor contamination of the komatiite magma during crystallization. However, a strong correlation between water contents of the trapped melts with the composition of the host high-Mg olivines (>92 Fo), consistent with closed-system fractionation argues against contamination at an early stage of crystallization. Thus, the excessive contents of H_2O, as well as Cl and F, estimated for the less-evolved melt likely represent those of the primary magma and hence its mantle source.

In this case two scenarios are possible: a supra-subduction origin of the komatiite melts (Grove et al., 1997; Parman et al., 1997; Parman et al., 2004) or derivation from a hydrous mantle plume (Shimizu et al., 2001; Sobolev et al., 2016). As shown on Fig. 11, the calculated parental melt for Zimbabwe komatiites has a smooth and flat trace-element pattern with

moderate depletion in the LREE, a strong negative Pb anomaly, and large positive H, Cl and F anomalies. The absence of typical supra-subduction features such as negative Nb-Ta anomalies and positive anomalies of large ion lithophile elements (Rb, Ba, K, Sr) and Pb suggests a non-subduction origin of both komatiites, as argued previously for Belingwe by McDonough and Ireland (1993) and Shimizu et al. (2001). While the subduction related geochemical fingerprints (e.g. negative Nb-Ta anomalies) do in fact exist in the Archean ultramafic and mafic volcanic rocks (Polat et al., 2010). The low oxygen fugacity of primary melts (lower than QFM- 1) also argues against a supra-subduction setting. Instead, these observations support a hydrous mantle plume origin of Belingwe komatiite as in the model recently proposed by Sobolev et al. (2016). In this model, the mantle transition zone between 410-660 km contained significant amounts of H_2O, F and Cl (Roberge et al., 2015; Roberge et al., 2017) which contaminated the plume en route to the lithosphere.

Sobolev et al. (2016) inferred 0.6 wt.% H_2O in the initial melts of 2.7 Ga Abitibi komatiites, a slightly higher value than inferred for the Belingwe melt. On the other hand, the H_2O/Ce ratio of the estimated primary melt is more than 6 times higher and Cl/K ratio is 13 times higher than those estimated ratios for modern depleted mantle. This difference probably reflects heterogeneous distribution of H_2O and Cl in the transition zone and/or differing extents of entrainment of hydrous material into the mantle plume

6.6. **Magma generation conditions**

Our estimated initial melt composition (Table 2) has MgO=27.5±2.9wt% and a liquidus temperature of 1513±54°C (2 standard errors). Magma generation pressures and temperatures were calculated using the method of Lee et al. (2009), which takes into account the presence of water and gives 1787°±54°C at 6.7±0.2 GPa or 223±6.7 (2 standard errors) km depth. These estimates correspond to 60% of partial melting, however, the initial melting depth was probably much deeper and could have started in the transition zone of mantle (410-660 km depth or >13 GPa), which allows mantle plume to entrain the transition zone material (Sobolev et al., 2016). The temperatures of the contemporary 2.7 Ga ambient mantle are estimated to be ~1600°C according to Korenaga (2008) and Herzberg et al. (2010) or 1500°C according to Ganne and Feng (2017). Thus, the calculated magma generation temperatures are at least 150 to 300°C hotter than ambient Archean mantle providing further evidence of a plume origin of Belingwe komatiites (McDonough and Ireland, 1993; Puchtel et al., 2009; Shimizu et al., 2001).

7. Concluding remarks

- Excess concentrations of Na_2O, CaO, Li, La, Cu, Rb, Y, Sc as well as of H_2O, Cl, F and S over the olivine fractionation line in the evolved trapped melts suggest contamination of the komatiite lava at shallow levels of during emplacement.
- No signs of contamination are observed for the melts hosted in the most magnesium rich olivines. Hence, these melts are representative of the parental komatiite magma.
- Belingwe komatiite lavas contained up to 23.5 wt.% MgO and 0.3 wt.% H_2O when they erupted. The parental melt was more magnesian, with up to 27.5 wt.% MgO. It contained ~0.2 wt. of water and had a liquidus temperature of 1513°C.
- Estimates of the parental melt water contents obtained directly by the SIMS analyses of melt inclusions are consistent with those obtained indirectly using the Sc/Y olivine-melt and Al-in-olivine-spinel geothermometers.
- The high H_2O and Cl contents estimated in the parental komatiite melt are thought to result from interaction of a mantle plume with a hydrous mantle transition zone.

Acknowledgments

This research was supported by the Russian Science Foundation grant number 14-17-00491 (to Sobolev A.V.). The EPMA facility in ISTerre was established and maintained by funds of the Agence Nationale de la Recherche, France, the Chair of Excellence grant ANR-09-CEXC-003-01 and partly by CNRS and Labex OSUG@2020 (Investissements d'avenir—ANR10 LABX56). The costs of SIMS analyses were covered by CRPG (AAG internal funds). This is CRPG contribution #2542. We thank V. Magnin for assistance in maintenance of the EPMA laboratory, U. Westernströer for help with laser-ablation ICP-MS measurements, C. Chauvel and S. Campillo for help with solution ICP-MS measurements.

References

Allègre, C.J., 1982. Genesis of Archaean komatiites in a wet ultramafic subducted plate. In: Arndt, N.T., Nisbet, E.G. (Ed.), Komatiites. George Allen and Unwin, London, pp. 495-500.

Arndt, N., Ginibre, C., Chauvel, C., Albarede, F., Cheadle, M., Herzberg, C., Jenner, G., Lahaye, Y., 1998. Were komatiites wet? Geology, 26(8): 739-742.

Arndt, N.T., Lesher, C.M., Barnes, S.J., 2008. Komatiite. Cambridge University Press, Cambridge, 466 pp.

Ballhaus, C., Berry, R., Green, D., 1991. High pressure experimental calibration of the olivine-orthopyroxene-spinel oxygen geobarometer: implications for the oxidation state of the upper mantle. Contributions to Mineralogy and Petrology, 107(1): 27-40.

Barnes, S.J., 1998. Chromite in komatiites, 1. Magmatic controls on crystallization and composition. Journal of Petrology, 39(10): 1689-1720.

Batanova, V.G., Belousov, I.A., Savelieva, G.N., Sobolev, A.V., 2011. Consequences of Channelized and Diffuse Melt Transport in Supra-subduction Zone Mantle: Evidence from the Voykar Ophiolite (Polar Urals). Journal of Petrology, 52(12): 2483-2521.

Batanova, V.G., Sobolev, A.V., Kuzmin, D.V., 2015. Trace element analysis of olivine: High precision analytical method for JEOL JXA-8230 electron probe microanalyser. Chemical Geology, 419: 149-157.

Berry, A.J., Danyushevsky, L.V., O'Neill, H.S.C., Newville, M., Sutton, S.R., 2008. Oxidation state of iron in komatiitic melt inclusions indicates hot Archaean mantle. Nature, 455(7215): 960-963.

Bickle, M., Arndt, N., Nisbet, E., Orpen, J., Martin, A., Keays, R., Renner, R., 1993. Geochemistry of the igneous rocks of the Belingwe greenstone belt: alteration, contamination and petrogenesis. The Geology of the Belingwe Greenstone Belt, Zimbabwe: 175-213.

Bickle, M.J., Ford, C.E., Nisbet, E.G., 1977. Petrogenesis of peridotitic komatiites - evidence from high-pressure melting experiments. Earth and Planetary Science Letters, 37(1): 97-106.

Bickle, M.J., Martin, A., Nisbet, E.G., 1975. Basaltic and peridotitic komatiites and stromatolites above a basal unconformity in belingwe greenstone belt, rhodesia. Earth and Planetary Science Letters, 27(2): 155-162.

Brooks, C., Hart, S., 1974. On the significance of komatiite. Geology, 2(2): 107-110.

Brown, P.E., 1989. FLINCOR; a microcomputer program for the reduction and investigation of fluid-inclusion data. American Mineralogist, 74(11-12): 1390-1393.

Campbell, I.H., Griffiths, R.W., Hill, R.I., 1989. Melting in an Archean mantle plume - heads its basalts, tails its komatiites. Nature, 339(6227): 697-699.

Chauvel, C., Bureau, S., Poggi, C., 2011. Comprehensive Chemical and Isotopic Analyses of Basalt and Sediment Reference Materials. Geostandards and Geoanalytical Research, 35(1): 125-143.

Chauvel, C., Dupré, B., Arndt, N., 1993. Pb and Nd isotopic correlation in Belingwe komatiites and basalts. The Geology of the Belingwe Greenstone Belt, Zimbabwe: Geological Society of Zimbabwe, Special Publication, 2: 167-174.

Connolly, B.D., Puchtel, I.S., Walker, R.J., Arevalo, R., Piccoli, P.M., Byerly, G., Robin-Popieul, C., Arndt, N., 2011. Highly siderophile element systematics of the 3.3 Ga Weltevreden komatiites, South Africa: implications for early Earth history. Earth and Planetary Science Letters, 311(3): 253-263.

Coogan, L.A., Saunders, A.D., Wilson, R.N., 2014. Aluminum-in-olivine thermometry of primitive basalts: Evidence of an anomalously hot mantle source for large igneous provinces. Chemical Geology, 368(0): 1-10.

Danyushevsky, L.V., Gee, M.A.M., Nisbet, E.G., Cheadle, M.J., 2002. Olivine-hosted melt inclusions in Belingwe komatiites: Implications for cooling history, parental magma composition and its H2O content. Geochimica Et Cosmochimica Acta, 66(15A): A168-A168.

Danyushevsky, L.V., Plechov, P., 2011. Petrolog3: Integrated software for modeling crystallization processes. Geochemistry Geophysics Geosystems, 12.

Dixon, J.E., Stolper, E.M., Holloway, J.R., 1995. An experimental study of water and carbon dioxide solubilities in mid-ocean ridge basaltic liquids. Part I: calibration and solubility models. Journal of Petrology, 36(6): 1607-1631.

Dupre, B., Arndt, N.T., 1990. Pb isotopic compositions of Archean komatiites and sulfides. Chemical Geology, 85(1-2): 35-56.

Esposito, R., Bodnar, R., Danyushevsky, L., De Vivo, B., Fedele, L., Hunter, J., Lima, A., Shimizu, N., 2011. Volatile evolution of magma associated with the Solchiaro eruption in the Phlegrean Volcanic District (Italy). Journal of Petrology, 52(12): 2431-2460.

Falloon, T.J., Danyushevsky, L.V., 2000. Melting of refractory mantle at 1.5, 2 and 2.5 GPa under, anhydrous and H2O-undersaturated conditions: Implications for the petrogenesis of high-Ca boninites and the influence of subduction components on mantle melting. Journal of Petrology, 41(2): 257-283.

Ford, C.E., Russell, D.G., Craven, J.A., Fisk, M.R., 1983. Olivine liquid equilibria - temperature, pressure and composition dependence of the crystal liquid cation partition-coefficients for Mg, Fe-2+, Ca and Mn. Journal of Petrology, 24(3): 256-265.

Ganne, J., Feng, X., 2017. Primary magmas and mantle temperatures through time. Geochemistry, Geophysics, Geosystems, 18(3): 872-888.

Grove, T., De Wit, M., Dann, J., 1997. Komatiites from the komati type section, Barberton, South Africa. Oxford monographs on geology and geophysics, 35(1): 438-456.

Gurenko, A.A., Kamenetsky, V.S., 2011. Boron isotopic composition of olivine-hosted melt inclusions from Gorgona komatiites, Colombia: New evidence supporting wet komatiite origin. Earth and Planetary Science Letters, 312(1-2): 201-212.

Gurenko, A.A., Kamenetsky, V.S., Kerr, A.C., 2016. Oxygen isotopes and volatile contents of the Gorgona komatiites, Colombia: A confirmation of the deep mantle origin of H 2 O. Earth and Planetary Science Letters, 454: 154-165.

Hartley, M.E., Maclennan, J., Edmonds, M., Thordarson, T., 2014. Reconstructing the deep CO 2 degassing behaviour of large basaltic fissure eruptions. Earth and Planetary Science Letters, 393: 120-131.

Herzberg, C., 2004. Geodynamic information in peridotite petrology. Journal of Petrology, 45(12): 2507-2530.

Herzberg, C., 2016. Petrological evidence from komatiites for an early Earth carbon and water cycle. Journal of Petrology, 57(11-12): 2271-2288.

Herzberg, C., Condie, K., Korenaga, J., 2010. Thermal history of the Earth and its petrological expression. Earth and Planetary Science Letters, 292(1-2): 79-88.

Herzberg, C., O'Hara, M.J., 2002. Plume-associated ultramafic magmas of phanerozoic age. Journal of Petrology, 43(10): 1857-1883.

Hirose, K., Kawamoto, T., 1995. Hydrous partial melting of lherzolite at 1 GPa: the effect of H2O on the genesis of basaltic magmas. Earth and Planetary Science Letters, 133(3-4): 463-473.

Hofmann, A.W., 1988. Chemical differentiation of the Earth: the relationship between mantle, continental crust, and oceanic crust. Earth Planet. Sci. Lett., 90: 297-314.

Inoue, T., 1994. Effect of water on melting phase relations and melt composition in the system Mg2SiO4・MgSiO3・H2O up to 15 GPa. Physics of the Earth and Planetary Interiors, 85(3-4): 237-263.

Inoue, T., Sawamoto, H., 1992. In High Pressure Research: Application to Earth and Planetary Sciences. Terrapub, Tokyo and AGU, Washington, DC: 323-331.

Jahn, B.-m., Gruau, G., Glikson, A., 1982. Komatiites of the Onverwacht Group, S. Africa: REE geochemistry, Sm/Nd age and mantle evolution. Contributions to Mineralogy and Petrology, 80(1): 25-40.

Jarosevich, E.J., Nelen, J.A., Norberg, J.A., 1980. Reference sample fro electron microprobe analysis. Geostand. Newsl., 4: 43-47.

Jochum, K., Arndt, N., Hofmann, A., 1991. Nb-Th-La in komatiites and basalts: constraints on komatiite petrogenesis and mantle evolution. Earth and Planetary Science Letters, 107(2): 272-289.

Jochum, K.P. et al., 2006. MPI-DING reference glasses for in situ microanalysis: New reference values for element concentrations and isotope ratios. Geochemistry Geophysics Geosystems, 7.

Kawamoto, T., Hervig, R.L., Holloway, J.R., 1996. Experimental evidence for a hydrous transition zone in the early Earth's mantle. Earth and Planetary Science Letters, 142(3-4): 587-592.

Kendrick, M., Hémond, C., Kamenetsky, V., Danyushevsky, L., Devey, C.W., Rodemann, T., Jackson, M., Perfit, M., 2017. Seawater cycled throughout Earth/'s mantle in partially serpentinized lithosphere. Nature Geoscience.

Kent, A.J., Peate, D.W., Newman, S., Stolper, E.M., Pearce, J.A., 2002. Chlorine in submarine glasses from the Lau Basin: seawater contamination and constraints on the composition of slab-derived fluids. Earth and Planetary Science Letters, 202(2): 361-377.

Kent, A.J.R., Norman, M.D., Hutcheon, I.D., Stolper, E.M., 1999. Assimilation of seawater-derived components in an oceanic volcano: evidence from matrix glasses and glass inclusions from Loihi seamount, Hawaii. Chemical Geology, 156(1-4): 299-319.

Kodolányi, J., Pettke, T., Spandler, C., Kamber, B.S., Gméling, K., 2011. Geochemistry of ocean floor and fore-arc serpentinites: constraints on the ultramafic input to subduction zones. Journal of Petrology, 53(2): 235-270.

Korenaga, J., 2008. Urey ratio and the structure and evolution of Earth's mantle. Reviews of Geophysics, 46(2).

Krasheninnikov, S.P., Sobolev, A.V., Batanova, V.G., Kargaltsev, A.A., Borisov, A.A., 2017. Experimental testing of olivine–melt equilibrium models at high temperatures. Doklady Earth Sciences, 475: 919-922.

Lassiter, J., Hauri, E., Nikogosian, I., Barsczus, H., 2002. Chlorine–potassium variations in melt inclusions from Raivavae and Rapa, Austral Islands: constraints on chlorine recycling in the mantle and evidence for brine-induced melting of oceanic crust. Earth and Planetary Science Letters, 202(3): 525-540.

Lee, C.-T.A., Luffi, P., Plank, T., Dalton, H., Leeman, W.P., 2009. Constraints on the depths and temperatures of basaltic magma generation on Earth and other terrestrial planets using new thermobarometers for mafic magmas. Earth and Planetary Science Letters, 279(1): 20-33.

Mallmann, G., O'Neill, H.S., 2013. Calibration of an Empirical Thermometer and Oxybarometer based on the Partitioning of Sc, Y and V between Olivine and Silicate Melt. Journal of Petrology, 54(5): 933-949.

McDonough, W.F., Ireland, T.R., 1993. Intraplate origin of komatiites inferred from trace-elements in glass inclusions. Nature, 365(6445): 432-434.

Mei, S., Kohlstedt, D., 2000. Influence of water on plastic deformation of olivine aggregates: 1. Diffusion creep regime. Journal of Geophysical Research: Solid Earth, 105(B9): 21457-21469.

Michael, P.J., Cornell, W.C., 1998. Influence of spreading rate and magma supply on crystallization and assimilation beneath mid-ocean ridges: Evidence from chlorine and major element chemistry of mid-ocean ridge basalts. Journal of Geophysical Research: Solid Earth, 103(B8): 18325-18356.

Milman-Barris, M.S., Beckett, J.R., Baker, M.B., Hofmann, A.E., Morgan, Z., Crowley, M.R., Vielzeuf, D., Stolper, E., 2008. Zoning of phosphorus in igneous olivine. Contributions to Mineralogy and Petrology, 155(6): 739-765.

Mironov, N., Portnyagin, M., Botcharnikov, R., Gurenko, A., Hoernle, K., Holtz, F., 2015. Quantification of the CO 2 budget and H 2 O–CO 2 systematics in subduction-zone magmas through the experimental hydration of melt inclusions in olivine at high H 2 O pressure. Earth and Planetary Science Letters, 425: 1-11.

Moore, L.R., Gazel, E., Tuohy, R., Lloyd, A.S., Esposito, R., Steele-MacInnis, M., Hauri, E.H., Wallace, P.J., Plank, T., Bodnar, R.J., 2015. Bubbles matter: An assessment of the

contribution of vapor bubbles to melt inclusion volatile budgets. American Mineralogist, 100(4): 806-823.

Nesbitt, R.W., Sun, S.-S., 1976. Geochemistry of Archaean spinifex-textured peridotites and magnesian and low-magnesian tholeiites. Earth and Planetary Science Letters, 31(3): 433-453.

Newman, S., Lowenstern, J.B., 2002. VOLATILECALC: a silicate melt-H2O-CO2 solution model written in Visual Basic for excel. Computers & Geosciences, 28(5): 597-604.

Nisbet, E.G., Arndt, N.T., Bickle, M.J., Cameron, W.E., Chauvel, C., Cheadle, M., Hegner, E., Kyser, T.K., Martin, A., Renner, R., Roedder, E., 1987. Uniquely fresh 2.7 ga komatiites from the Belingwe greenstone-belt, Zimbabwe. Geology, 15(12): 1147-1150.

Nisbet, E.G., Bickle, M.J., Martin, A., 1977. Mafic and ultramafic lavas of Belingwe greenstone belt, Rhodesia. Journal of Petrology, 18(4): 521-566.

Parman, S.W., Dann, J.C., Grove, T.L., deWit, M.J., 1997. Emplacement conditions of komatiite magmas from the 3.49 Ga Komati Formation, Barberton Greenstone Belt, South Africa. Earth and Planetary Science Letters, 150(3-4): 303-323.

Parman, S.W., Grove, T.L., Dann, J.C., de Wit, M.J., 2004. A subduction origin for komatiites and cratonic lithospheric mantle. South African Journal of Geology, 107(1-2): 107-118.

Polat, A., Appel, P.W., Fryer, B.J., 2011. An overview of the geochemistry of Eoarchean to Mesoarchean ultramafic to mafic volcanic rocks, SW Greenland: implications for mantle depletion and petrogenetic processes at subduction zones in the early Earth. Gondwana Research, 20(2): 255-283.

Portnyagin, M., Almeev, R., Matveev, S., Holtz, F., 2008. Experimental evidence for rapid water exchange between melt inclusions in olivine and host magma. Earth and Planetary Science Letters, 272(3-4): 541-552.

Puchtel, I.S., Walker, R.J., Brandon, A.D., Nisbet, E.G., 2009. Pt-Re-Os and Sm-Nd isotope and HSE and REE systematics of the 2.7 Ga Belingwe and Abitibi komatiites. Geochimica Et Cosmochimica Acta, 73(20): 6367-6389.

Renner, R., Nisbet, E.G., Cheadle, M.J., Arndt, N.T., Bickle, M.J., Cameron, W.E., 1994. Komatiite flows from the reliance formation, Belingwe belt, Zimbabwe .1. Petrography and mineralogy. Journal of Petrology, 35(2): 361-400.

Roberge, M., Bureau, H., Bolfan-Casanova, N., Frost, D.J., Raepsaet, C., Surble, S., Khodja, H., Auzende, A.-L., Fiquet, G., 2015. Is the transition zone a deep reservoir for fluorine? Earth and Planetary Science Letters, 429: 25-32.

Roberge, M., Bureau, H., Bolfan-Casanova, N., Raepsaet, C., Surble, S., Khodja, H., Auzende, A.-L., Cordier, P., Fiquet, G., 2017. Chlorine in wadsleyite and ringwoodite: An experimental study. Earth and Planetary Science Letters, 467: 99-107.

Rosenthal, A., Hauri, E., Hirschmann, M., 2015. Experimental determination of C, F, and H partitioning between mantle minerals and carbonated basalt, CO 2/Ba and CO 2/Nb systematics of partial melting, and the CO 2 contents of basaltic source regions. Earth and Planetary Science Letters, 412: 77-87.

Ruscitto, D.M., Wallace, P.J., Cooper, L.B., Plank, T., 2012. Global variations in H2O/Ce: 2. Relationships to arc magma geochemistry and volatile fluxes. Geochemistry, Geophysics, Geosystems, 13(3).

Shimizu, K., Komiya, T., Hirose, K., Shimizu, N., Maruyama, S., 2001. Cr-spinel, an excellent micro-container for retaining primitive melts - implications for a hydrous plume origin for komatiites. Earth and Planetary Science Letters, 189(3-4): 177-188.

Shimizu, K., Nakamura, E., Maruyama, S., 2005. The geochemistry of ultramafic to mafic volcanics from the Belingwe Greenstone Belt, Zimbabwe: magmatism in an Archean continental large igneous province. Journal of Petrology, 46(11): 2367-2394.

Sobolev, A.V., Asafov, E.V., Gurenko, A.A., Arndt, N.T., Batanova, V.G., Portnyagin, M.V., Garbe-Schonberg, D., Krasheninnikov, S.P., 2016. Komatiites reveal a hydrous Archaean deep-mantle reservoir. Nature, 531(7596): 628-632.

Sobolev, A.V., Danyushevsky, L.V., 1994. Petrology and geochemistry of boninites from the North termination of the Tonga trench - constraints on the generation conditions of primary high-ca boninite magmas. Journal of Petrology, 35(5): 1183-1211.

Sobolev, A.V. et al., 2007. The amount of recycled crust in sources of mantle-derived melts. Science, 316(5823): 412-417.

Steele-Macinnis, M., Esposito, R., Bodnar, R.J., 2011. Thermodynamic model for the effect of post-entrapment crystallization on the H2O–CO2 systematics of vapor-saturated, silicate melt inclusions. Journal of Petrology, 52(12): 2461-2482.

Stiegler, M.T., Cooper, M., Byerly, G.R., Lowe, D.R., 2012. Geochemistry and petrology of komatiites of the Pioneer Ultramafic Complex of the 3.3 Ga Weltevreden Formation, Barberton greenstone belt, South Africa. Precambrian Research, 212: 1-12.

Stone, W.E., Deloule, E., Larson, M.S., Lesher, C.M., 1997. Evidence for hydrous high-MgO melts in the Precambrian. Geology, 25(2): 143-146.

Wallace, P.J., Kamenetsky, V.S., Cervantes, P., 2015. Melt inclusion CO2 contents, pressures of olivine crystallization, and the problem of shrinkage bubbles. American Mineralogist, 100(4): 787-794.

Walter, M.J., 1998. Melting of garnet peridotite and the origin of komatiite and depleted lithosphere. Journal of Petrology, 39(1): 29-60.

Figure Captions

Fig. 1. Geological map of Belingwe Greenstone Belt, south-central Zimbabwe (modified after Shimizu et al., 2005). Analyzed samples z6 and z4 come from Tony's Flow, Belingwe

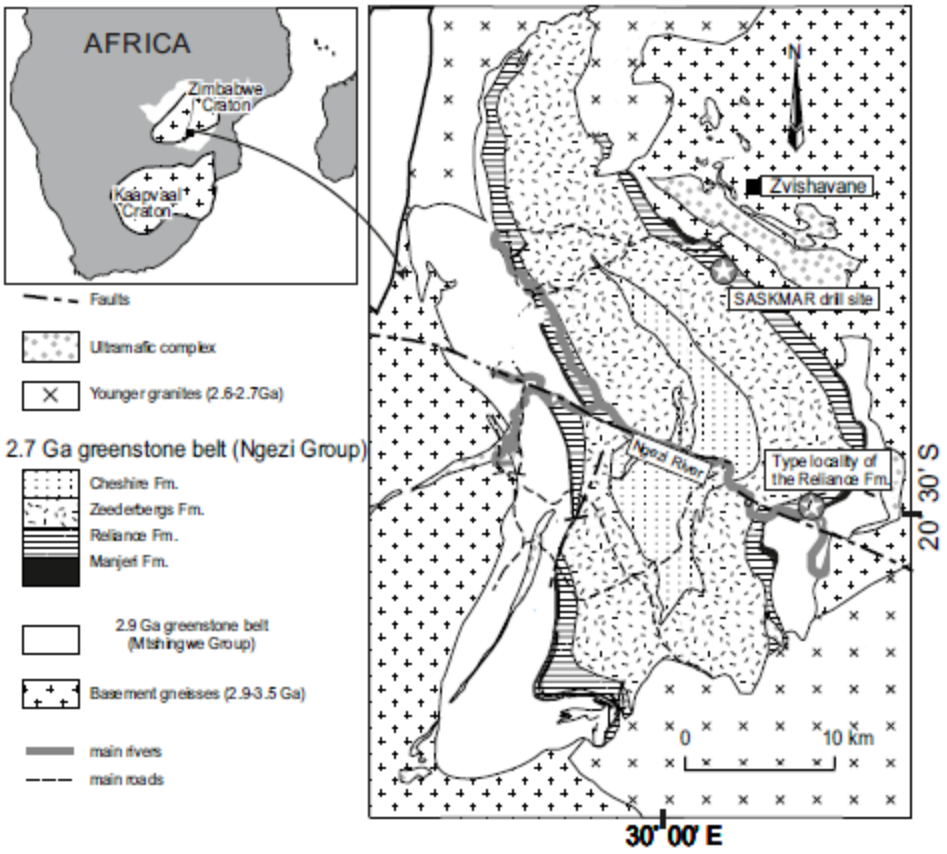

Fig.1

Fig. 2. Melt inclusions in olivine from Belingwe belt komatiite z6. A,b,c – heated and quenched inclusions in the transmitted light; d – unheated inclusion hosted in the olivine in the thin section, back scattered electron image. Inclusions contain glass and a gas bubble, b inclusions also contains spinel crystal.

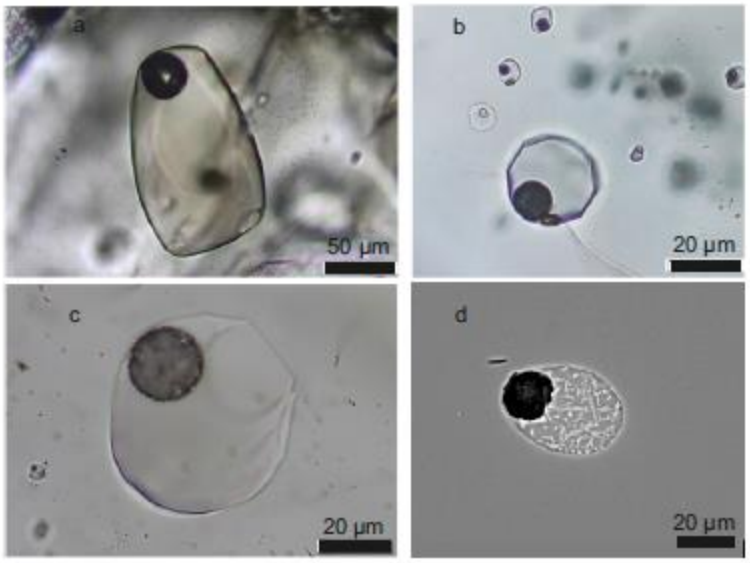

Fig. 2.

Fig. 3. Major element compositions of olivine from the Z4 and Z6 olivine cumulates. Black arrows display the crystallizing phases. Cr_2O_3 demonstrates the start of the spinel crystallization when olivine has the composition Fo91.

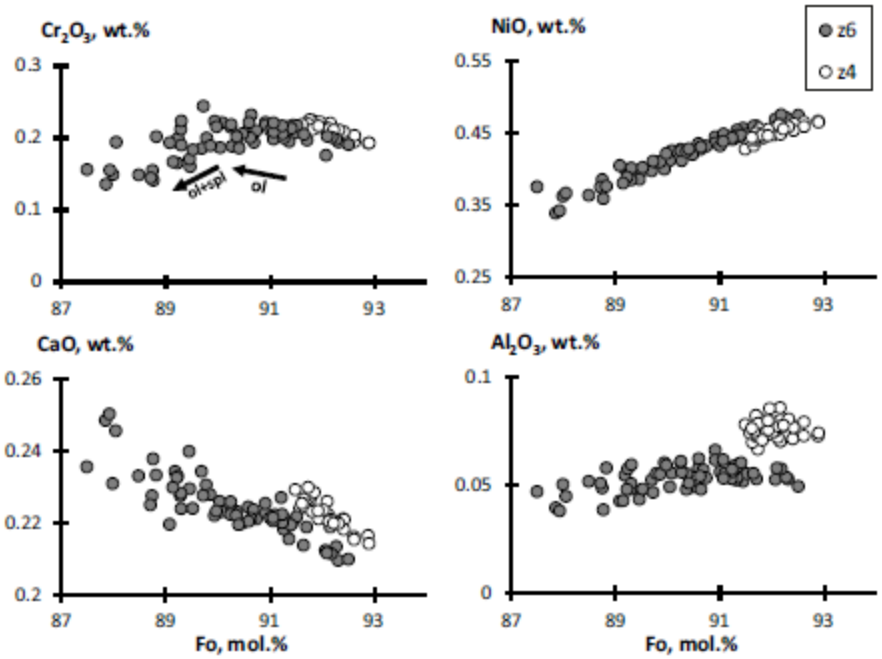

Fig.3.

Fig. 4. Back scattered image and element qualitative distribution maps for the olivine grain in the thin section of Z6 komatiite. Normal magmatic shape and original magmatic zoning in Cr, Al and P provide evidence that the olivine grains escaped post-magmatic alteration and retain the originally trapped melts. The approximate concentrations of elements are reproduced in the color scales.

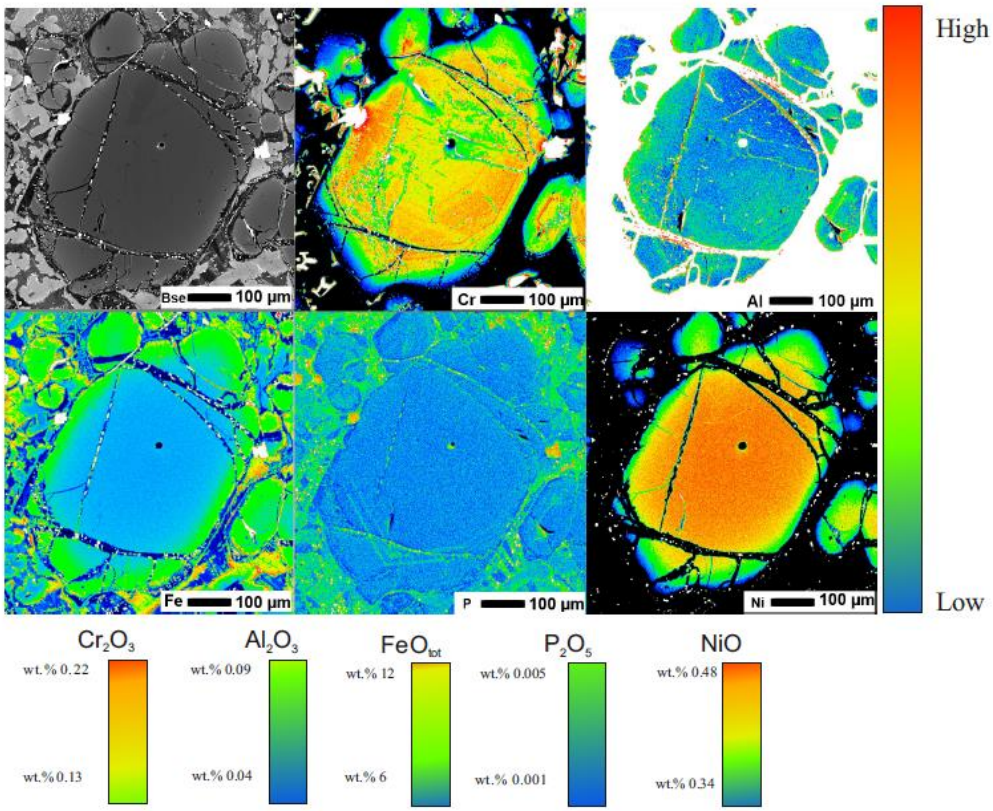

Fig. 4.

Fig. 5. Compositions of melt inclusions. Literature data from Nisbet et al., 1987, Bickle et al., 1993, Shimizu et al., 2005, Puchtel et al., 2009). Z6-Cl - chlorine rich melt inclusion; wr (Z, ZV, TN) – whole rock data. Some samples are out of scale

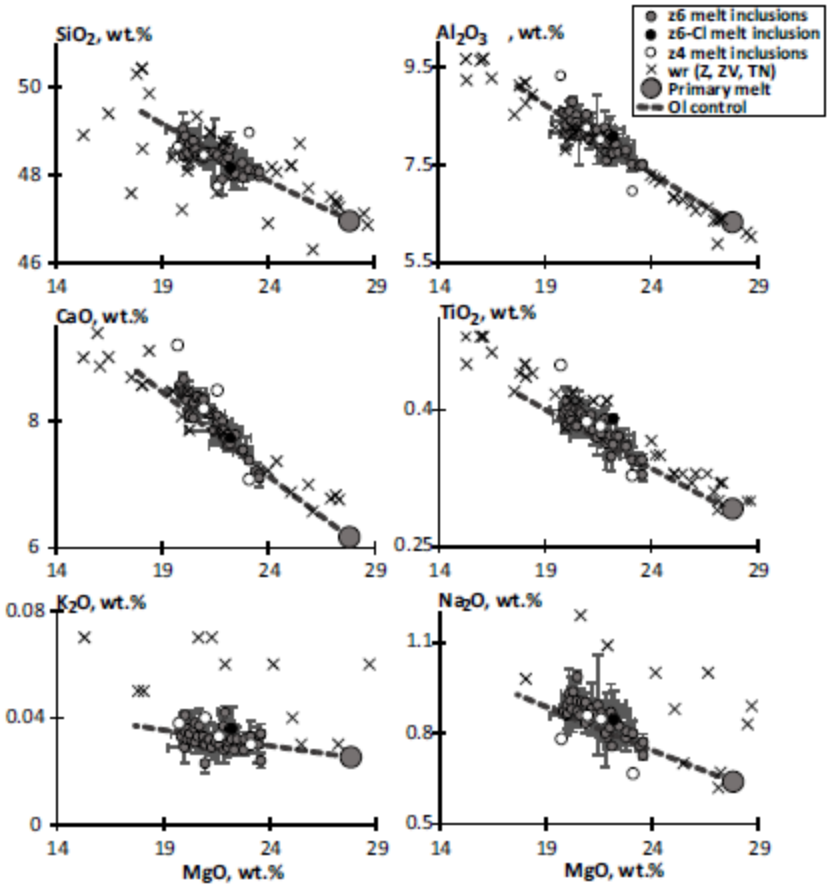

Fig. 5.

Fig. 6. Trace element contents of melt inclusions. z6-Cl – melt inclusion with extremely high Cl; wr (Z, ZV, TN) – whole rock data from literature (Nisbet et al., 1987, Bickle et al., 1993, Shimizu et al., 2005, Puchtel et al., 2009), some samples are out of scale. Sc demonstrates a systematic shift compared to the whole rock data due to the redistribution into the host olivine. Sc and Rb plot away from the olivine control line and were affected by the AFC process. Y, Ba and Ce follow the olivine control line within the error. Z6-Cl - chlorine rich melt inclusion is consistent with the melt inclusions data set. For Sc, V and Y – whole rock samples are more representative for the primary melt (see Section 4.6 for methods and Section 6.2 for discussion).

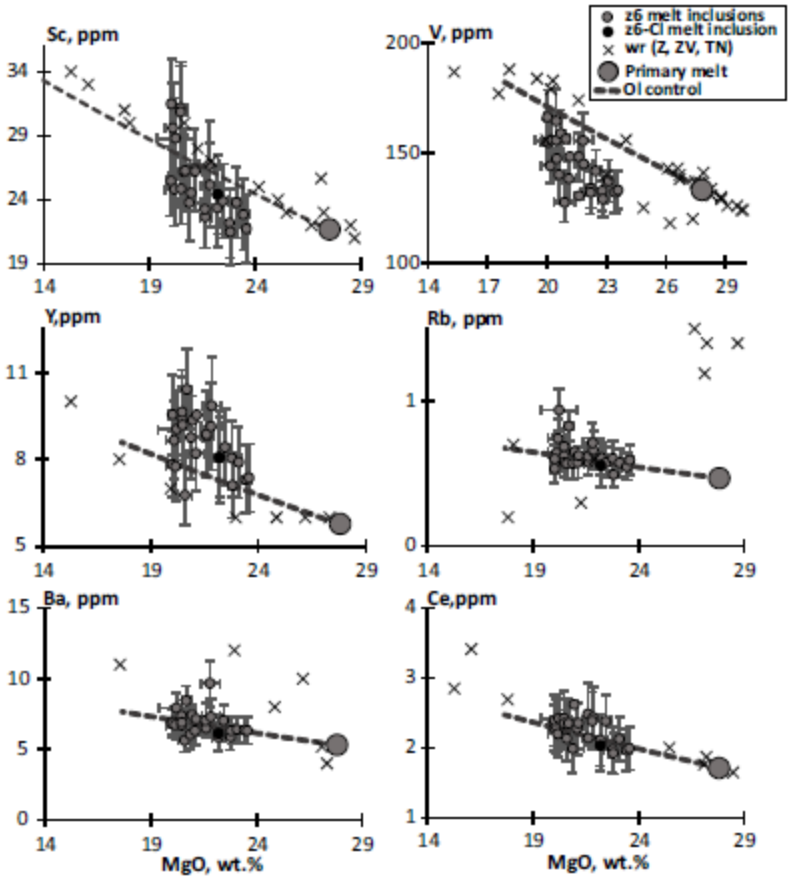

Fig.6.

Fig. 7. Spider diagram of melt inclusions and Tony flow whole rock samples normalized to 0.39 wt.% TiO_2 (average for the trapped melt inclusions). All data normalized for the incompatible lithophile elements in the primitive mantle after Hofmann (1988). Water, fluorine and chlorine were estimated from the ratios of H_2O/Ce=166, Cl/K=0.10, F/Nd=22.7. Average ratios for uncontaminated OIB and MORB glasses after Kendrick et al. (2017).Whole rock data from Bickle et al. (1993). Grey shaded field – range of the trapped melt compositions.

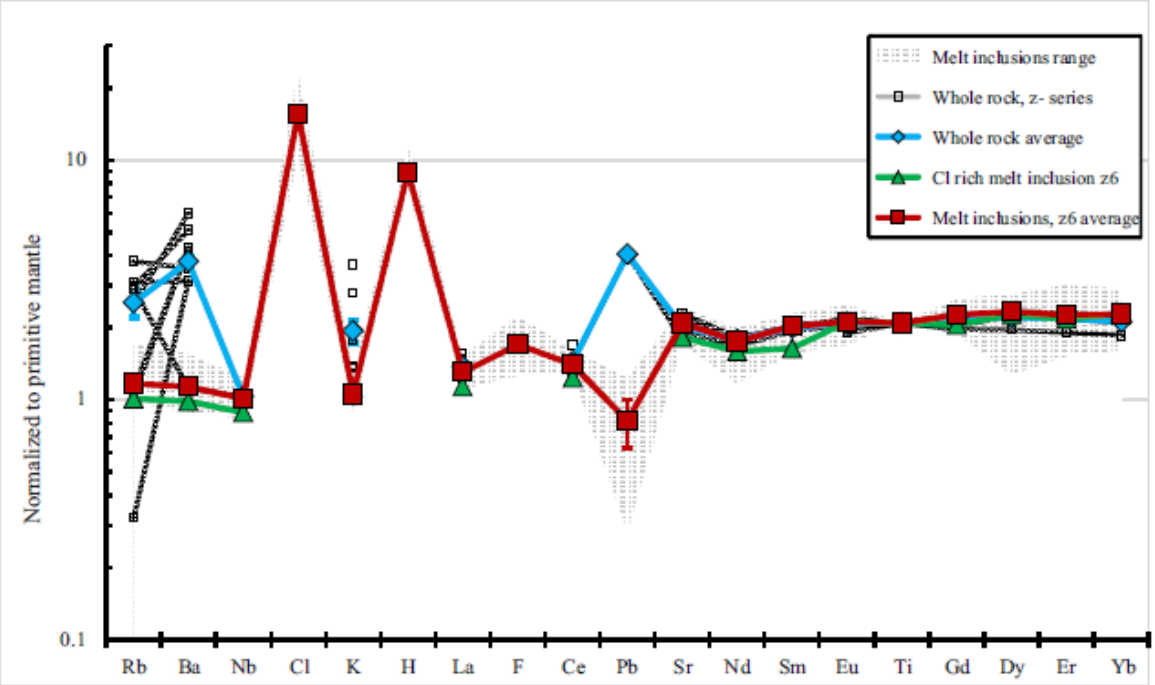

Fig. 7.

Fig. 8. Volatile contents in the melt inclusions. Data show correlation with the forsterite content of the olivine but the slopes are steeper than the olivine control line.

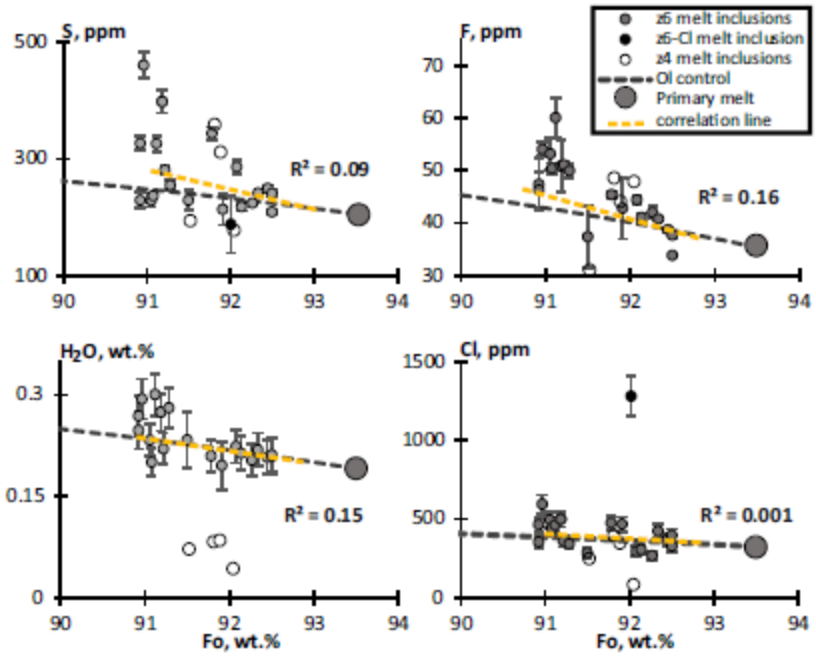

Fig. 8.

Fig. 9. Water contents versus Cl, S, F and size of the melt inclusions. Mi – melt inclusions; Corr – correlation lines. Correlations between H_2O and other volatiles suggest that melt inclusions did not lose or gain water after the entrapment and represent the initial magma contents. The absence of a correlation with the size of olivine grains provides strong evidence again diffusion of H_2O.

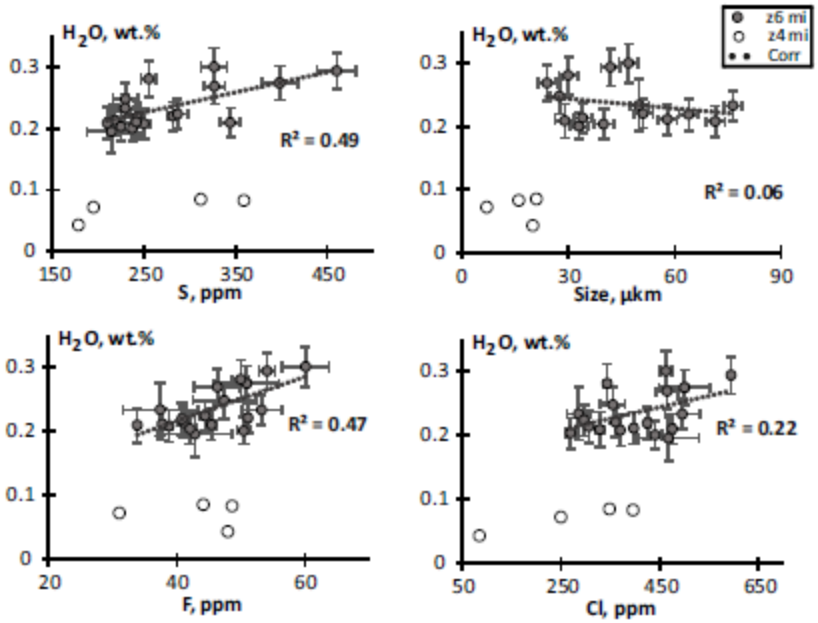

Fig. 9.

Fig. 10. Pressure calculated using the measured and corrected. Dashed line – average pressure- is given for the corrected CO_2 contents of the trapped melts (Newman and Lowenstern, 2002) refer to the depth of crystallization of the host olivine.

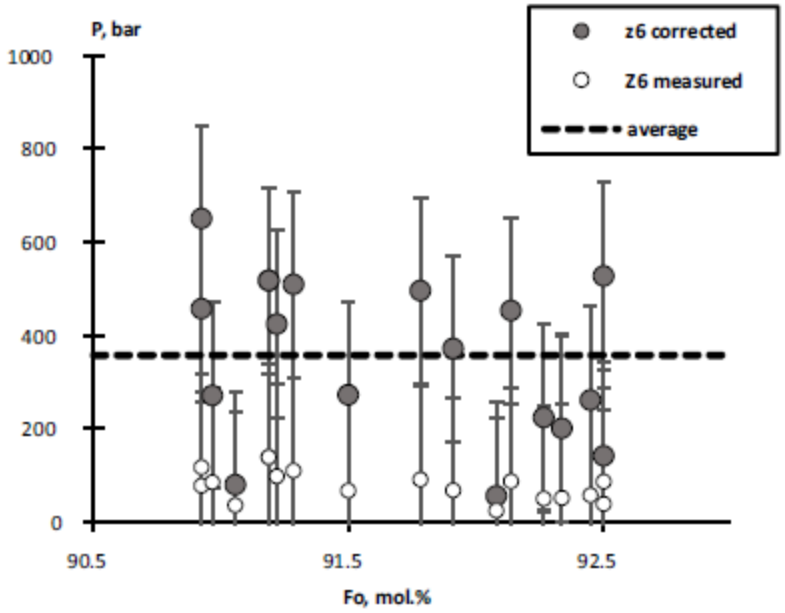

Fig. 10.

Fig. 11. A. Crystallization temperatures of Belingwe komatiites versus olivine composition. Temperatures are estimated from Sc/Y olivine-melt, Mg-Fe olivine-melt and Al olivine-spinel geothermometers (See Methods).Dashed lines show liquidus temperatures of the komatiite melt with various water contents. B. Oxygen fugacity, estimated from V partitioning between olivine and melt, follows a closed-system trend.

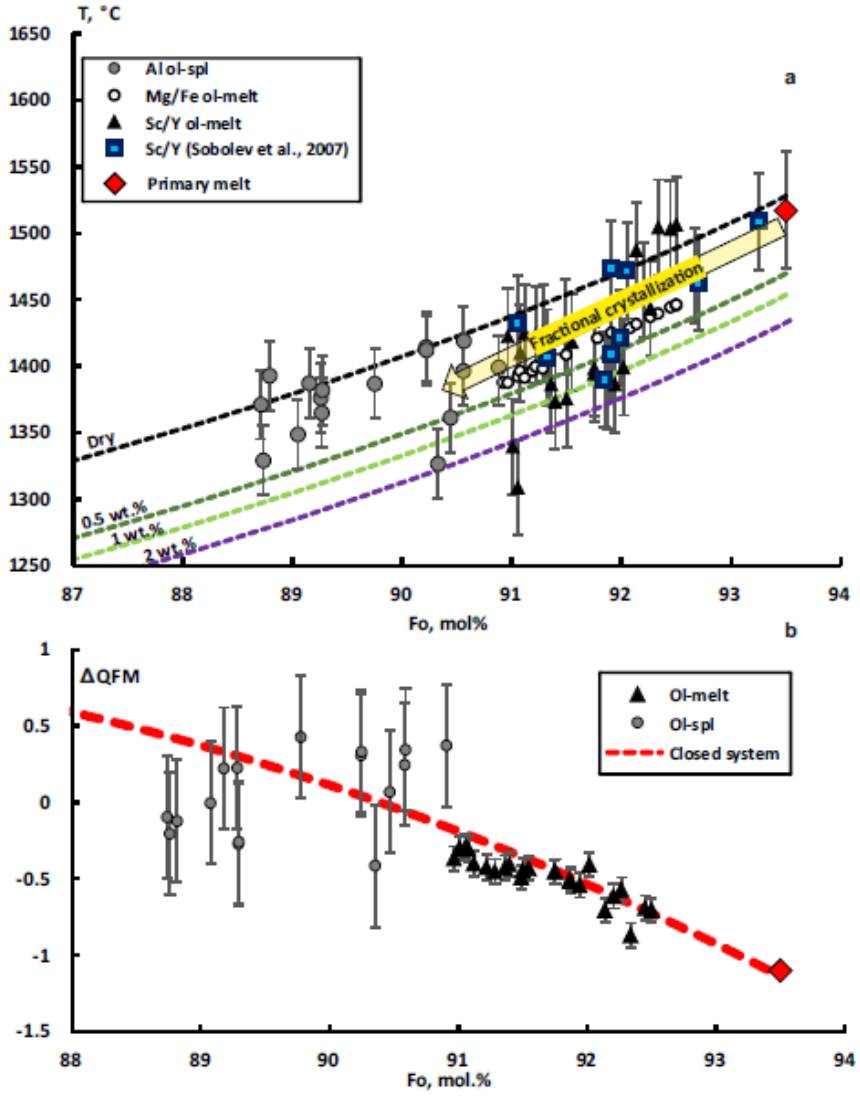

Fig. 11.

Fig. 12. H_2O/Cl versus K/Cl with melt inclusions data for Belingwe komatiites (this study), Abitibi komatiites (Sobolev et al., 2016) and Gorgona komatiites (Gurenko and Kamenetsky, 2011; Gurenko et al., 2016). Arc lavas – the primitive magma compositions compilation by Ruscitto et al. (2012). MORB and OIB glasses compilation by Kendrick et al. (2017). "Contaminated" identifies samples that may have assimilated seawater Cl. AOC – altered oceanic crust (Michael and Cornell, 1998). Serpentine data from(Kodolányi et al., 2011)

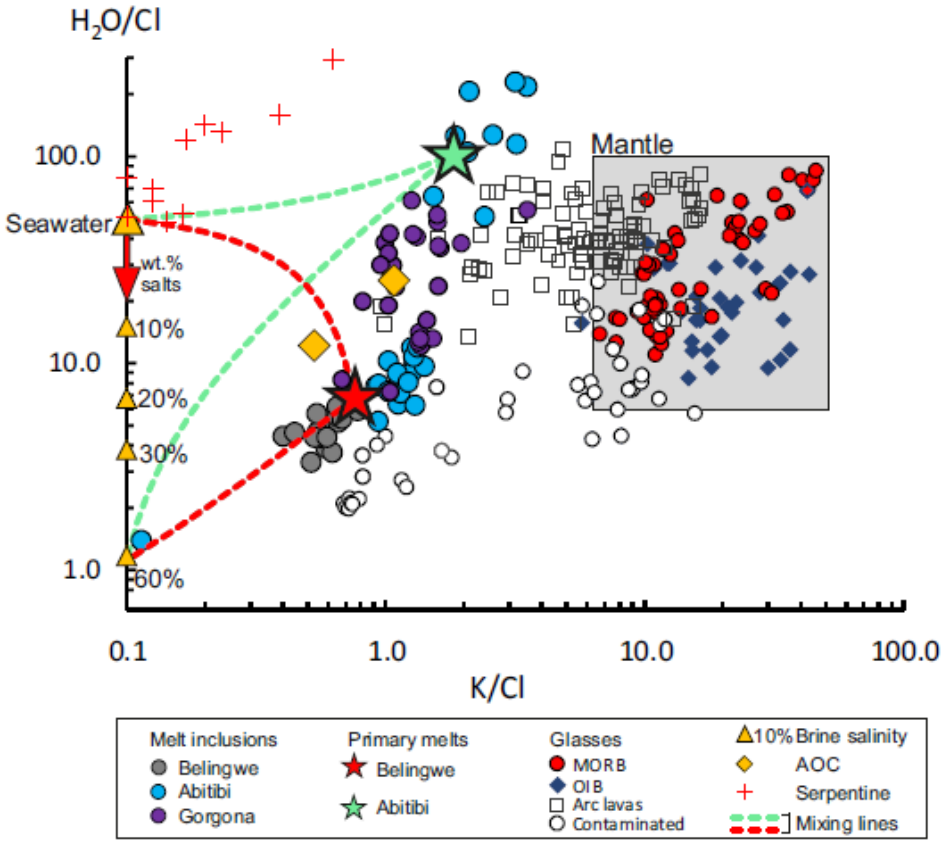

Fig. 12.

Fig. 13. MgO and SiO_2 contents of komatiites from Belingwe (this study) and Abitibi (Sobolev et l., 2016) komatiites compared with the model volatile-free primary magmas of peridotite KR4003 produced by batch melting (a) and accumulated fractional melting (b) after Herzberg (2016).

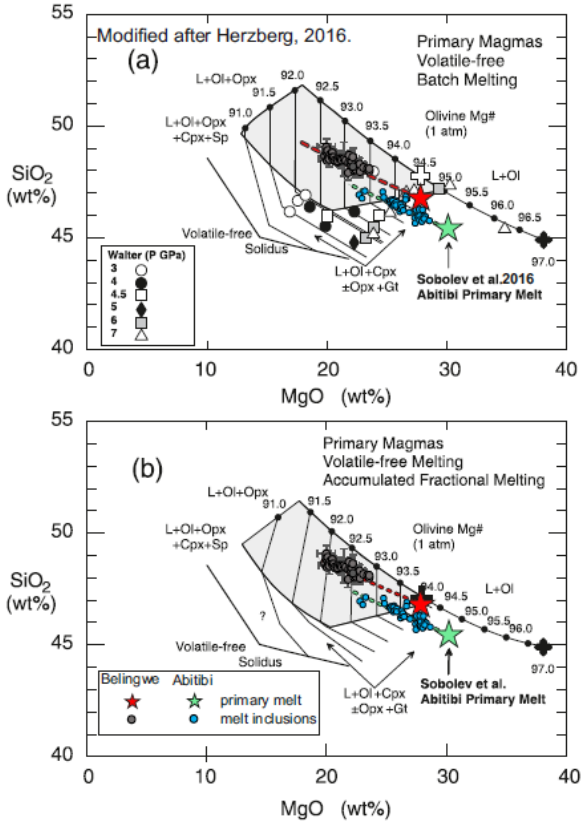

Fig. 13.

Fig. 14. Spider diagram of the calculated parental melt for z6 komatiites and parental melt for the Abitibi komatiites inferred from the melt inclusions (Sobolev et al., 2016). Knowing the approximate degree of partial melting (60%) and assuming olivine with minor ortopyroxene to be the only residual phases in the restite allows to reconstruct the source peridotite trace element composition by roughly multiplying the initial komatiite melt composition by 0.6 All data normalized for the incompatible lithophile elements in the PM after Hofmann (1988). Water, fluorine and chlorine were estimated from the ratios of H2O/Ce=166, Cl/K=0.10, F/Nd=22.7. Average ratios for uncontaminated OIB and MORB glasses after Kendrick et al. (2017).

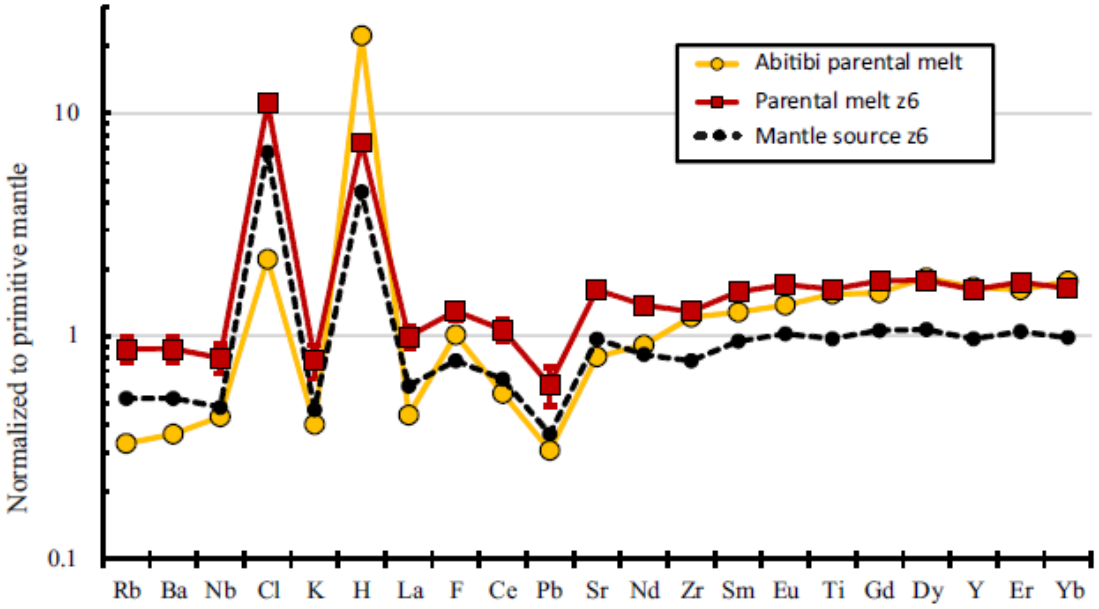

Fig. 14.

Table captions

Table 1. Representative compositions of olivine from the samples z6 and z4 analyzed by the EPMA. Concentrations are given in wt.%.

SAMP_NO	z6ol67	z6ol68	z6ol69	z6ol70	z4
z6ol1					
z6ol2					
z6ol3					
z6ol4					
z6ol5					
z6ol6					
z6ol7					
z6ol9					
z6ol10					
z6ol11					
z6ol13					
z6ol14					
z6ol15					
z6ol16					
z6ol17					
z6ol18					
z6ol19					
z6ol20					
z6ol21					
z6ol22					
z6ol23					
z6ol24					
z6ol25					
z6ol26					
z6ol27					
z6ol28					
z6ol29					
z6ol30					
z6ol31					
z6ol32					
z6ol33					
z6ol35					
z6ol36					
z6ol37					
z6ol38					
z6ol39					
z6ol41					
z6ol42					
z6ol43					
z6ol44					
z6ol46					
z6ol47					
z6ol48					
z6ol49					
z6ol50					
z6ol51					
z6ol52					
z6ol53					
z6ol54					
z6ol55					
z6ol57					
z6ol58					
z6ol59					
z6ol60					
z6ol61					
z6ol62					
z6ol63					
z6ol64					
z6ol65					
z6ol66					

o
l
1

z
4

o
l
2

z
4

o
l
3

z
4

o
l
4

z
4

o
l
5

z
4

o
l
6

z
4

o
l
8

z
4

o
l
9

z
4

o
l
1
2

z
4

o
l
1
4

z
4

o
l
1
5

z
4

o
l
1
6

z
4

o
l
1
7

z
4

o
l
1
8

z
4

o
l
1
9

z
4

o
l
2
0

z
4

o
l
2
1

z
4

o
l
2
2

z
4

o
l
2
3

z
4

o
l
2
4

z
4

o
l
2
5

z
4

o
l
2
6

z
4

o
l
2
7

z
4

o
l
2
8

z
4

o
l
2
9

z
4

ol30

z4

ol31

z4

ol32

z4

ol33

z4

o
l
3
5

z
4

o
l
3
6

z
4

o
l
3
7

z
4

o
l
3
8

z
4

3 7 5 0 6 8 6 1 6 4 1 9 1 9 8 9 2 1 8 1 7 4 1 6 4 3 8 2 6 0 5 0 4 8 3 2 9 6 7 3 3 4 3 0 4 9 8 8 5 5 6 5 5 2 1 0 7 2 2 7

92.18

89.14

92.09

91.78

91.85

91

.
4
8

9
2
.
0
1

9
2
.
1
6

9
2
.
1
5

9
2
.
1
9

9
1
.
9

92.11

92.06

92.42

91.65

92.61

92

.
8
8

9
1
.
6
2

9
1
.
7
0

9
2
.
8
9

9
2
.
0
2

9
1
.
7

2

92.17

92.41

91.81

91.57

91.92

91.66

91.73

92.13

92.32

92.22

91

.81

91.92

91.61

0.005

0.004

0.005

Na_2O	0.005	0.006	0.007	0.007	0.008	0.008	0.005	0.006	0.005	0.007	0.004	0.005	0.006	0.006	0.006	0.006	0.005	0.006	0.007	0.005	0.006	0.005	0.007	0.005	0.006	0.006	0.007	0.006	0.004	0.006	0.004	0.006	0.005	0.005	0.005	0.005	0.006	0.006	0.004	0.004	0.005	0.004	0.007	0.005	0.005	0.006	0.007	0.006	0.006	0.005	0.007	0.003	0.004	0.004	0.007	0.005	0.005	0.005	0.006	0.005	0.

0.078

0.078

0.073

0.071

0.086

0.

0
7
7

0
.
0
8
6

0
.
0
7
9

0
.
0
7
0

0
.
0
7
2

0
.
0
7

3

0.0822

0.0722

0.0755

0.0777

0.0777

0.079

0.073

0.070

0.073

0.074

0.

0
7
5

0
.
0
7
3

0
.
0
8
0

0
.
0
7
7

0
.
0
7
7

0
.
0
7

4

0.076

0.075

0.079

0.077

0.081

2
2
8

0
.
2
2
9

0
.
2
2
3

0
.
2
2
1

0
.
2
1
9

0
.
2
2

1

0.223

0.226

0.219

0.221

0.216

0.224

0.222

0.221

0.221

0.227

0.

2
1
5

0
.
2
1
6

0
.
2
2
5

0
.
2
2
5

0
.
2
1
4

0
.
2
2

3

0.2255

0.2211

0.2188

0.2233

0.2244

0.221

0.225

0.230

0.220

0.220

0.

P_2O_5	0.003	0.001	0.004	0.002	0.002	0.003	0.003	0.003	0.004	0.002	0.002	0.002	0.001	0.002	0.004	0.002	0.004	0.002	0.002	0.002	0.002	0.002	0.002	0.003	0.004	0.001	0.004	0.001	0.002	0.001	0.002	0.002	0.002	0.004	0.002	0.003	0.002	0.002	0.001	0.003	0.003	0.003	0.002	0.001	0.002	0.004	0.002	0.003	0.005	0.001	0.003	0.004	0.003	0.003	0.002	0.002	0.002	0.002	0.002	0.004

220

0.223

0.223

0.225

0.002

0.003

0.

0.443

0.445

0.428

0.450

0.458

0.

4
6
2

0
.
4
5
9

0
.
4
5
2

0
.
4
6
0

0
.
4
6
1

0
.
4
6

0

0.466

0.451

0.460

0.452

0.463

0.433

0.460

0.467

0.448

0.451

0.

4
6
6

0
.
4
4
8

0
.
4
4
1

0
.
4
4
9

0
.
4
5
4

0
.
4
4

4

0
.
4
4
4
1

0
.
4
5
6

0
.
4
4
2

0
.
4
4
6

0
.
4
6
2

2 3 3 3 2 4 4 2 3 4 3 2 4 3 1 4 3 2 3 3 3 4 2 5 2 3 4 3 3 3 4 2 3 3 3 2 3 3 2 3 3 3 4 3 4 5 3 3 4 4 4 3 4 2 4 3 3 3 3 4 3 0.004

0.003

0.004

0.004

0.004

0.

0
0
4

0
.
0
0
4

0
.
0
0
2

0
.
0
0
5

0
.
0
0
3

0
.
0
0

3

0
.
0
0
3

0
.
0
0
2

0
.
0
0
3

0
.
0
0
3

0
.
0
0
3

0.003

0.004

0.003

0.003

0.003

0.

0
0
2

0
.
0
0
4

0
.
0
0
4

0
.
0
0
4

0
.
0
0
3

0
.
0
0

3

0.0044

0.0022

0.0033

0.0033

0.0033

0.003

0.004

0.004

0.003

0.005

0.

1
2
6

0
.
1
2
7

0
.
1
2
5

0
.
1
3
1

0
.
1
2
3

0
.
1
1
1

9

0
.
1
1
9

0
.
1
2
0

0
.
1
2
5

0
.
1
2
1

0
.
1
2
3

0.116

0.114

0.127

0.121

0.120

0.

1
1
6

0
.
1
2
9

0
.
1
1
3

0
.
1
0
8

0
.
1
2
6

0
.
1
2

6

0.1090

0.1211

0.1255

0.1200

0.1188

0.126

0.127

0.124

0.127

0.128

0.

1
2
0

0
.
1
1
7

0
.
1
1
8

0
.
1
2
5

0
.
1
2
3

0
.
1
2

3

0.2155

0.2188

0.2066

0.2211

0.2088

0.222

0.211

0.208

0.200

0.195

0.

3

0.1933

0.2166

0.2144

0.1933

0.2144

0.216

0.211

0.209

0.215

0.215

0.

2
1
5

0
.
2
1
4

0
.
2
2
0

0
.
2
1
3

0
.
2
1
1

0
.
2
1

8

50.87

50.37

50.38

49.95

50.45

50.55

50.82

50.69

50.45

50.51

50

.
8
7

5
0
.
5
1

5
1
.
0
7

5
0
.
8
7

5
0
.
8
1

4
9
.
8

0

50.79

50.46

51.11

50.95

49.52

49.83

51.07

50.30

49.65

50.86

51

.
5
6

5
0
.
3
1

4
9
.
6
6

5
0
.
8
9

5
0
.
1
6

5
0
.
6

6

50.64

50.98

50.67

50.60

50.86

7.73

7.72

7.41

7.27

8.22

7.76

7.

66

7.42

8.20

7.27

6.96

8.07

8.04

6.96

7.78

7.99

7.71

7.55

8.00

8

.
1
5

7
.
9
7

8
.
1
3

8
.
1
4

7
.
7
2

7
.
5
6

7
.
6

1.26

41.26

41.25

41.12

41.28

41.

41.13

41.38

41.68

41.49

40.96

4

1.31

41.35

41.36

41.16

40.59

40.

78

41.20

41.11

40.81

41.31

41.88

41.25

40.72

41.65

41.21

41.74

4

1.08

41.34

41.08

41.34

41.33

40.

		9
		1000.70
		1000.44
		1000.62
		1000.56
		10

		1.03
		1000.71
		1000.72
		1000.50
		1011.08

	100.12
	1000.79
	101.87
	101.14
	99.

		50
		1000.61
		1011.09
		1000.81
		1000.139

		99.26
		99.74
		100.29
		100.27
		99.54
		1

		0 0 . 9 7
		1 0 2 . 0 7
		1 0 0 . 6 4
		9 9 . 6 2
		1 0 1 . 6 1

		100.59
		101.64
		100.52
		100.97
		100

		. 4 6
		1 0 1 . 0 6
		1 0 1 . 2 5
		9 9 . 8 3

Table 2. Melt inclusions corrected data on the major and trace element concentrations and volatile contents and calculated parental melt compositions.

	SAMP_NO	Size, μm	EPMA, wt.% SiO_2	TiO_2
	MZ-4ol1*	-48	48.42	0.379
	MZ-4ol2*	-48	48.27	0.372
	MZ-4ol3*	-47	47.99	0.357
	MZ-4ol4*	-47	47.96	0.355
	MZ-4ol5*	-47	47.95	0.355
	MZ-4ol6*	-47	47.91	0.352
	MZ-4ol7*	-47	47.88	0.351
	MZ-4ol8*	-47	47.54	0.333
	MZ-4ol9*	-47	47.53	0.332
	MZ-4ol10*	-47	47.22	0.316
	z6-Cl1[1]	24	48.17	0.390
	z6-2		48.38	0.387
	z6-23	27	48.45	0.397
	z6-24	24	48.49	0.400
	z6-25	41	48.82	0.382
	z6-26		48.89	0.404
	z6-27	38	48.45	0.410
	z6-28	76	48.58	0.393
	z6-29	33	48.57	0.397
	z6-30		48.71	0.397
	z6-10	47	48.51	0.388
	z6-11	250	48.79	0.401
	z6-12		48.79	0.384
	z6-13	51	48.58	0.382
	z6-14		48.59	0.398
	z6-15		48.44	0.396
	z6-16	46	48.49	0.392
	z6-17		48.43	0.388
	z6-18	47	48.41	0.388
	z6-19		48.53	0.380
	z6-20		48.52	0.394
	z6-21		48.46	0.378
	z6-22		48.52	0.370
	z6-23	58	48.43	0.374
	z6-24		48.46	0.385
	z6-25		48.67	0.363
	z6-26	30	48.35	0.389
	z6-27	40	48.47	0.390
	z6-28		48.48	0.367
	z6-29		48.44	0.372
	z6-30		48.49	0.349
	z6-31	35	48.54	0.362
	z6-32		48.47	0.372
	z6-33	34	48.44	0.371
	z6-34	34	48.55	0.363
	z6-35		48.49	0.360
	z6-36	46	48.44	0.345
	z6-37	71	48.54	0.343
	z6-38		48.47	0.345
	z6-39	29	48.47	0.329
	z4-1	58	48.48	0.449
	z4-2	16	48.64	0.482
	z4-3	21	48.47	0.487
	z4-4	74	48.46	0.482
		20	48.48	0.328
Average, Fo 92.1-92.5		48	48.70	0.351
Parental melt, Ford et al., 1983		47	47.37	0.313
Parental melt, Herzberg&O'Hara, 2002		46	46.20	0.279
Parental melt, average		47	47.00	0.296
		0	0.74	0.035

A																																																									
l	8	8	7	7	7	7	7	7	7	6	8	8	8	8	8	8	8	8	8	8		8	8	8	8	8	8	8	8	8	8	8	8	7	7	7	8	8	8	7	7	7	7	7	7	7	7	7	7	9	8	8	6	7	6	6	6	0
2	.	.	.	.	.	.	.	.	.	.	.	.	.	.	.	.	.	.	.	.		.	.	.	.	.	.	.	.	.	.	.	.	.	.	.	.	.	.	.	.	.	.	.	.	.	.	.	.	.	.	.	.	.	.	.	.	.
O	2	0	7	7	7	6	6	2	2	8	0	5	5	1	3	1	5	6	8	4		5	3	1	1	1	3	3	0	2	2	2	0	9	6	9	2	1	0	7	7	9	7	7	8	5	4	5	5	3	0	2	9	6	8	0	4	7
3	3	6	3	0	0	5	1	3	1	6	8	3	8	5	3	2	4	0	0	0	8.15	2	7	1	6	8	1	1	2	0	3	3	5	2	0	4	6	3	2	3	3	3	6	5	0	1	8	2	0	3	2	6	7	2	2	6	4	6
F																																																									
e	1	1	1	1	1	1	1	1	1	1	1	1	1	1	1	1	1	1	1	1		1	1	1	1	1	1	1	1	1	1	1	1	1	1	1	1	1	1	1	1	1	1	1	1	1	1	1	1	1	1	1	1	1	1	0	0	0
2	.	.	.	.	.	.	.	.	.	.	.	.	.	.	.	.	.	.	.	.		.	.	.	.	.	.	.	.	.	.	.	.	.	.	.	.	.	.	.	.	.	.	.	.	.	.	.	.	.	.	.	.	.	.	.	.	.
O	3	3	2	2	2	2	2	1	1	1	2	2	2	2	2	2	2	2	2	2		2	2	2	2	2	2	2	2	2	2	2	2	2	2	2	2	2	2	2	2	1	1	1	1	1	1	1	1	1	2	2	2	1	0	9	9	1
3	4	1	6	5	5	5	4	8	7	2	0	5	9	9	9	9	8	8	8	8	1.27	7	7	6	6	5	5	4	4	4	4	3	2	2	2	1	1	1	1	1	1	9	9	8	8	7	6	6	6	1	1	3	1	7	5	2	9	2
	1	1	1	1	1	1	1	1	1	1	1	1	1	1	1	1	1	1	1	1		1	1	1	1	1	1	1	1	1	1	1	1	1	1	1	1	1	1	1	1	1	1	1	1	1	1	1	1	1	1	1	1	1	1	1	1	
	1	1	1	1	1	1	1	0	0	0	0	1	1	1	1	1	1	1	1	1		1	1	1	1	1	1	1	1	1	1	1	1	1	0	0	0	0	0	0	0	0	0	0	0	0	0	0	0	0	0	0	1	0	0	0	0	0
F	.	.	.	.	.	.	.	.	.	.	.	.	.	.	.	.	.	.	.	.		.	.	.	.	.	.	.	.	.	.	.	.	.	.	.	.	.	.	.	.	.	.	.	.	.	.	.	.	.	.	.	.	.	.	.	.	.
e	3	3	1	1	1	1	1	9	9	7	9	0	1	1	1	0	0	0	0	0	11.0	0	0	0	0	0	0	0	0	0	0	0	0	0	9	9	9	9	9	9	9	9	9	9	9	8	8	8	8	0	9	9	0	8	4	1	2	3
O	6	1	9	8	8	6	4	5	3	2	5	4	0	0	0	9	9	8	8	8	8	7	7	6	6	5	4	4	3	3	2	1	0	0	9	8	8	7	7	7	6	4	2	1	0	8	5	4	4	1	9	5	6	8	7	2	9	5
	0	0	0	0	0	0	0	0	0	0	0	0	0	0	0	0	0	0	0	0		0	0	0	0	0	0	0	0	0	0	0	0	0	0	0	0	0	0	0	0	0	0	0	0	0	0	0	0	0	0	0	0	0	0	0	0	0
	.	.	.	.	.	.	.	.	.	.	.	.	.	.	.	.	.	.	.	.		.	.	.	.	.	.	.	.	.	.	.	.	.	.	.	.	.	.	.	.	.	.	.	.	.	.	.	.	.	.	.	.	.	.	.	.	.
M	1	1	1	1	1	1	1	1	1	1	1	1	1	1	1	1	1	1	1	1		1	1	1	1	1	1	1	1	1	1	1	1	1	1	1	1	1	1	1	1	1	1	1	1	1	1	1	1	1	1	2	1	1	1	1	1	0
n	3	3	3	3	3	3	3	3	3	2	2	2	2	2	3	2	3	2	2	2	0.13	2	1	2	2	2	2	2	2	2	2	2	2	2	2	2	4	2	1	2	2	1	1	2	1	2	2	1	0	9	9	0	8	1	1	0	1	0
O	5	4	3	3	3	3	3	0	0	8	2	2	9	2	6	8	6	8	9	1	6	9	4	2	0	2	1	1	1	8	9	2	9	9	1	2	3	8	6	1	2	4	5	2	5	1	1	5	8	1	1	1	1	7	6	8	2	8
	2	2	2	2	2	2	2	2	2	2	2	2	1	1	2	2	2	2	2	2		2	2	2	2	2	2	2	2	2	2	2	2	2	2	2	2	2	2	2	2	2	2	2	2	2	2	2	2	1	2	2	2	2	2	2	2	
	0	1	2	2	2	2	3	4	4	5	2	0	9	9	0	0	0	0	0	0		0	0	0	0	0	0	0	1	1	1	1	1	1	1	1	1	2	2	2	2	2	2	2	3	3	3	3	9	1	0	3	3	6	8	7	2
M	.	.	.	.	.	.	.	.	.	.	.	.	.	.	.	.	.	.	.	.		.	.	.	.	.	.	.	.	.	.	.	.	.	.	.	.	.	.	.	.	.	.	.	.	.	.	.	.	.	.	.	.	.	.	.	.	.
g	8	4	6	7	7	9	0	4	5	7	2	9	8	9	0	1	0	1	3	2	20.4	4	4	6	6	8	8	9	1	1	2	4	6	6	9	8	8	0	0	1	2	3	4	7	8	1	4	5	5	7	6	9	1	1	0	9	5	9
O	2	3	1	4	4	3	7	6	3	9	2	5	5	9	2	1	3	8	0	4	7	8	9	1	9	9	9	7	1	6	7	6	3	1	0	6	2	2	8	2	1	4	6	8	2	1	4	8	8	4	1	7	1	1	7	9	3	1
	7	7	7	7	7	7	7	7	7	6	7	8	8	8	8	8	8	8	8	8		8	8	8	8	8	8	8	8	8	8	7	7	8	7	8	7	7	7	7	7	7	7	7	7	7	7	7	7	9	8	8	7	7	6	5	6	0
C	.	.	.	.	.	.	.	.	.	.	.	.	.	.	.	.	.	.	.	.		.	.	.	.	.	.	.	.	.	.	.	.	.	.	.	.	.	.	.	.	.	.	.	.	.	.	.	.	.	.	.	.	.	.	.	.	.
a	9	8	5	5	5	4	4	0	0	6	7	2	5	4	4	3	6	3	1	4		0	3	3	3	2	3	3	1	1	1	8	9	0	7	0	8	7	6	7	6	7	7	5	5	3	2	1	1	2	4	2	0	3	6	8	2	7
O	7	2	4	1	1	6	2	6	3	8	4	0	7	8	2	9	8	4	0	7	8.27	5	0	8	9	2	6	4	5	5	2	6	9	9	9	0	8	4	3	9	5	5	9	4	5	9	1	7	1	1	9	0	8	9	4	8	6	5
	0	0	0	0	0	0	0	0	0	0	0	0	0	0	0	0	0	0	0	0		0	0	0	0	0	0	0	0	0	0	0	0	0	0	0	0	0	0	0	0	0	0	0	0	0	0	0	0	0	0	0	0	0	0	0	0	0
N	.	.	.	.	.	.	.	.	.	.	.	.	.	.	.	.	.	.	.	.		.	.	.	.	.	.	.	.	.	.	.	.	.	.	.	.	.	.	.	.	.	.	.	.	.	.	.	.	.	.	.	.	.	.	.	.	.
a	8	8	7	7	7	7	7	7	7	6	8	8	8	8	8	9	8	9	9	8		9	8	8	9	8	9	8	8	8	8	8	8	8	7	8	8	8	8	7	8	8	8	7	8	7	7	7	7	7	8	8	6	7	6	6	6	0
2	3	1	8	7	7	7	7	3	2	9	4	4	7	5	9	3	6	0	3	8	0.90	8	7	6	0	3	0	6	4	8	6	9	6	6	8	5	0	1	7	5	5	3	2	8	0	9	5	2	7	8	4	5	6	8	9	1	5	8
O	3	6	3	9	9	4	0	2	9	5	6	6	3	9	4	1	6	8	8	0	7	7	3	0	4	4	3	4	7	1	3	4	4	7	8	2	1	9	0	8	1	5	3	5	7	9	9	8	1	2	7	9	7	2	8	6	7	2
	0	0	0	0	0	0	0	0	0	0	0	0	0	0	0	0	0	0	0	0		0	0	0	0	0	0	0	0	0	0	0	0	0	0	0	0	0	0	0	0	0	0	0	0	0	0	0	0	0	0	0	0	0	0	0	0	0
	.	.	.	.	.	.	.	.	.	.	.	.	.	.	.	.	.	.	.	.		.	.	.	.	.	.	.	.	.	.	.	.	.	.	.	.	.	.	.	.	.	.	.	.	.	.	.	.	.	.	.	.	.	.	.	.	.
K	0	0	0	0	0	0	0	0	0	0	0	0	0	0	0	0	0	0	0	0		0	0	0	0	0	0	0	0	0	0	0	0	0	0	0	0	0	0	0	0	0	0	0	0	0	0	0	0	0	0	0	0	0	0	0	0	0
2	3	3	3	3	3	3	3	3	3	2	3	2	3	2	4	3	3	3	3	3	0.03	3	3	3	3	3	3	3	3	3	2	3	3	3	4	2	3	2	3	3	3	2	3	2	3	3	3	2	3	3	3	4	3	3	2	2	2	0
O	4	4	2	2	2	2	2	0	0	9	6	3	3	9	1	2	5	6	2	4	6	8	1	3	7	0	3	0	2	2	9	1	0	0	2	8	7	9	1	6	2	8	2	8	2	3	0	4	4	8	3	0	0	0	7	4	5	3
	0	0	0	0	0	0	0	0	0	0	0	0	0	0	0	0	0	0	0	0		0	0	0	0	0	0	0	0	0	0	0	0	0	0	0	0	0	0	0	0	0	0	0	0	0	0	0	0	0	0	0	0	0	0	0	0	0
P	.	.	.	.	.	.	.	.	.	.	.	.	.	.	.	.	.	.	.	.		.	.	.	.	.	.	.	.	.	.	.	.	.	.	.	.	.	.	.	.	.	.	.	.	.	.	.	.	.	.	.	.	.	.	.	.	.
2	0	0	0	0	0	0	0	0	0	0	0	0	0	0	0	0	0	0	0	0		0	0	0	0	0	0	0	0	0	0	0	0	0	0	0	0	0	0	0	0	0	0	0	0	0	0	0	0	0	0	0	0	0	0	0	0	0
O	2	2	2	2	2	2	2	2	2	1	3	1	2	0	2	2	3	3	2	3	0.02	3	3	2	1	2	3	3	2	2	1	3	3	2	2	2	2	2	1	2	2	2	1	2	1	2	2	4	1	2	1	2	3	2	1	1	1	0
5	3	2	1	1	1	1	1	0	0	9	0	1	8	8	8	3	0	9	2	1	7	8	1	2	9	6	0	1	0	1	6	5	4	8	0	5	4	6	7	7	4	8	9	6	1	0	2	0	7	7	8	5	3	2	8	6	7	2
C	0	0	0	0	0	0	0	0	0	0	0	0	0	0	0	0	0	0	0	0		0	0	0	0	0	0	0	0	0	0	0	0	0	0	0	0	0	0	0	0	0	0	0	0	0	0	0	0	0	0	0	0	0	0	0	0	0
r	.	.	.	.	.	.	.	.	.	.	.	.	.	.	.	.	.	.	.	.		.	.	.	.	.	.	.	.	.	.	.	.	.	.	.	.	.	.	.	.	.	.	.	.	.	.	.	.	.	.	.	.	.	.	.	.	.
2	2	2	2	2	2	2	2	2	2	2	2	2	2	2	2	2	2	2	2	2		2	2	2	2	2	2	2	2	2	2	2	2	2	2	2	2	2	2	2	2	2	2	2	2	2	2	2	2	3	3	3	3	2	2	1	2	0
O	4	4	3	3	3	3	3	2	2	1	2	5	3	4	5	7	3	3	2	5	0.18	4	5	5	5	5	4	6	5	5	5	4	4	6	5	5	4	4	4	5	5	3	4	4	4	4	4	5	2	7	6	3	1	4	2	9	1	2
3	5	2	6	5	5	4	3	6	6	9	6	0	6	7	7	0	1	5	8	9	5	1	0	2	2	9	9	2	9	9	4	6	9	0	2	0	2	8	2	4	6	8	3	6	3	2	7	1	9	9	6	7	0	3	4	9	2	6
											0	0	0	0	0	0	0	0	0	0	0.04	0	0	0	0	0	0	0	0	0	0	0	0	0	0	0	0	0	0	0	0	0	0	0	0	0	0	0	0	0	0	0	0	0	0	0	0	0
C											.	.	.	.	.	.	.	.	.	.	6	.	.	.	.	.	.	.	.	.	.	.	.	.	.	.	.	.	.	.	.	.	.	.	.	.	.	.	.	.	.	.	.	.	.	.	.	.

	l											128	032	046	061	063	052	045	052	042	053
	S											0.019	0.030	0.033	0.040	0.046	0.038	0.027	0.027	0.030	0.040
	Total	99.78	99.83	99.88	99.89	99.89	99.89	99.89	99.88	99.88	99.80	100.15	100.06	99.81	99.81	99.81	99.76	99.84	99.86	100.07	99.78
SIMS, ppm	H_2O, wt.%													0.25	0.27	0.29		0.23	0.20		0.30
	CO_2													209	300	121		34			
	F													47	46	54		53	50		60
	S													230	327	461		229	237		327
	Cl													355	465	595		495	441		462
LA-ICP-MS, ppm	Li											1.2				1.7	1.8	1.9	1.4		2.0
	Sc	28.5	27.9	26.9	26.8	26.8	26.6	26.5	25.2	25.1	24.0	24.4				25.5	29.6	31.5	24.8		28.8
	V	176.0	172.4	165.6	164.8	164.8	163.7	162.9	154.8	154.4	147.1	133.8				154.9	154.9	166.4	144.1		155.8

	l			058	040	039	065	038	066	041	036	047	040	039	063	052	057	047	061	038	053
	S	0.043		0.030	0.026	0.029	0.025	0.026	0.031	0.032	0.031	0.026	0.032	0.026	0.025	0.028	0.036	0.029	0.016	0.028	0.031
	Total	99.81		100.09	99.83	99.77	99.82	99.80	100.10	100.07	99.81	100.07	100.07	100.06	100.09	100.08	99.85	100.08	99.77	100.07	100.08
SIMS, ppm	H_2O, wt.%	0.27			0.22	0.28					0.23						0.21				
	CO_2	237			194	233					123						228				
	F	51			51	50					37						45				
	S	399			282	255					230						344				
	Cl	500			360	343					285						475				
LA-ICP-MS, ppm	Li	1.9	1.9		1.3	1.4	1.5	1.2		1.3	1.2	1.6			1.4	1.3		1.7	1.4		
	Sc	31.2	30.9		24.8	26.2	26.3	23.8		24.5	26.4	26.2			22.6	23.3		25.2	26.7		
	V	164.6	155.8		147.5	140.2	158.9	127.5		156.5	138.3	148.4			130.5	148.3		144.9	155.6		

	l	059	041	036	040	036	035	050	047	045	048	048	042	058	011	043	039	034	036	004
	S	0.020	0.025	0.034	0.029	0.032	0.025	0.032	0.027	0.027	0.028	0.046	0.039	0.042	0.024	0.029	0.026	0.023	0.024	0.003
	Total	99.85	100.07	99.82	99.82	100.07	99.82	99.83	99.82	99.80	99.83	100.01	100.00	100.03	99.99	99.86	99.88	99.89	99.88	
SIMS, ppm	H_2O, wt.%	0.20		0.22	0.21		0.20	0.22	0.21	0.21	0.21	0.08	0.09	0.07	0.04	0.21	0.19	0.17	0.18	0.02
	CO_2	170		23	208		101	90	118	243	63		116		55	137	123	109	116	14
	F	43		44	41		42	41	39	34	38	49	44	31	48	39	35	31	33	4
	S	214		287	218		225	242	250	210	242	359	312	195	178	231	207	184	195	23
	Cl	467		296	306		269	425	370	328	397	396	348	250	84	349	313	278	295	35
LA-ICP-MS, ppm	Li		1.1		1.5	1.5	1.1	1.1	1.4		1.1					1.1	1.14	1.01	1.1	0.1
	Sc		23.4		23.9	22.2	21.5	23.8	22.9		21.7					21.1	20.28	18.03	19.2	2.3
	V		132.0		141.9	132.8	129.1	137.2	132.2		133.0					119.7	120.32	106.92	113.6	13.4

																																					4	4		
											5	6	5	6	4	6	7	6	5	7	4	4	5	4	5	4	5	5	6	4	5	4	4	5	5	4	4	5	0	4	
											0	3	2	8	6	9	7	9	9	1	8	3	3	9	3	3	0	4	1	6	1	8	5	5	2	8	6	.	.	2	5
C											.	.	.	.	.	.	.	.	.	.	.	.	.	.	.	.	.	.	.	.	.	.	.	.	.	.	.	1	1	.	.
u											3	6	3	3	0	2	4	9	4	1	2	3	7	7	1	6	9	1	7	5	8	0	9	5	9	6	1	5	3	6	0
																																						0	0		
											0	0	0	0	0	0	0	0	0	0	0	0	0	0	0	0	0	0	0	0	0	0	0	0	0	0	0	.	.	0	0
R											.	.	.	.	.	.	.	.	.	.	.	.	.	.	.	.	.	.	.	.	.	.	.	.	.	.	.	5	4	.	.
b											6	5	6	6	7	9	7	6	6	6	8	6	7	6	6	6	6	7	7	6	6	6	5	6	5	6	5	1	5	5	1
																																						3	2		
											3	3	3	3	3	4	4	3	3	3	4	3	4	3	4	3	3	4	4	3	3	3	3	3	3	3	3	1	8	3	
											4	9	9	9	7	0	0	9	9	2	0	6	1	7	0	4	9	0	5	6	7	5	5	5	4	4	1	.	.	0	3
S											.	.	.	.	.	.	.	.	.	.	.	.	.	.	.	.	.	.	.	.	.	.	.	.	.	.	.	7	2	.	.
r											1	7	1	1	9	6	5	9	7	4	8	0	1	1	8	8	0	6	2	1	4	7	4	8	1	5	7	8	4	0	5
																					1																	6	6		
	6	6	5	5	5	5	5	5	4	4	8	7	8	9	7	9	9	9	9	6	0	8	9	8	9	8	8	9	9	8	8	8	7	7	7	7	7	.	.	6	0
	.	.	.	.	.	.	.	.	.	.	.	.	.	.	.	.	.	.	.	.	.	.	.	.	.	.	.	.	.	.	.	.	.	.	.	.	.	8	1	.	.
Y	8	5	9	8	8	7	7	0	9	3	1	8	7	5	8	1	4	6	2	8	4	8	4	2	5	8	9	9	1	1	4	0	1	9	3	4	1	9	2	5	8
																																						1	1		
											1	1	1	1	1	1	1	1	1	1	1	1	1	1	1	1	1	1	1	1	1	1	1	1	1	1	1	3	2	1	
											5	6	7	8	5	8	8	9	7	4	8	7	8	5	8	6	7	9	8	6	6	5	4	5	4	4	3	.	.	2	1
Z											.	.	.	.	.	.	.	.	.	.	.	.	.	.	.	.	.	.	.	.	.	.	.	.	.	.	.	5	0	.	.
r											9	4	2	6	1	1	7	0	6	5	8	2	7	6	6	2	7	9	3	0	6	6	3	7	3	4	9	5	4	8	5
											0	0	0	0	0	0	0	0	0	0	0	0	0	0	0	0	0	0	0	0	0	0	0	0	0	0	0	0	0	0	0
											.	.	.	.	.	.	.	.	.	.	.	.	.	.	.	.	.	.	.	.	.	.	.	.	.	.	.	.	.	.	.
N											5	6	6	6	6	6	7	6	6	5	6	5	7	5	7	5	6	6	6	5	7	5	6	5	5	5	5	5	4	5	0
b											6	5	6	2	8	5	0	3	4	4	5	8	1	9	5	8	8	7	2	2	5	6	1	7	4	4	3	3	7	0	6
											6	6	6	6	6	7	7	6	6	5	8	6	7	6	7	6	7	7	9	5	7	5	6	6	6	6	5	5	5	5	0
											.	.	.	.	.	.	.	.	.	.	.	.	.	.	.	.	.	.	.	.	.	.	.	.	.	.	.	.	.	.	.
B											1	9	9	8	7	9	3	7	9	6	4	0	4	3	1	5	0	3	6	8	0	8	3	4	3	3	5	7	0	4	6
a											4	4	3	4	3	3	8	1	0	3	4	5	3	3	4	0	5	0	8	7	5	9	3	0	6	3	2	3	9	1	4
											0	0	0	0	0	0	0	0	0	0	0	0	0	0	0	0	0	0	0	0	0	0	0	0	0	0	0	0	0	0	0
											.	.	.	.	.	.	.	.	.	.	.	.	.	.	.	.	.	.	.	.	.	.	.	.	.	.	.	.	.	.	.
L											7	7	8	8	7	8	9	7	8	7	9	7	9	7	8	7	9	8	8	7	8	7	6	7	6	7	6	6	5	6	0
a											2	5	4	2	9	8	0	8	8	1	5	2	5	7	8	8	0	2	4	1	6	4	9	4	9	0	7	6	9	2	7
											2	2	2	2	2	2	2	2	2	2	2	1	2	2	2	2	2	2	2	2	2	1	1	2	1	1	1	1	1	1	0
											.	.	.	.	.	.	.	.	.	.	.	.	.	.	.	.	.	.	.	.	.	.	.	.	.	.	.	.	.	.	.
C											0	2	3	3	2	4	4	3	3	1	3	9	6	2	3	1	4	4	3	1	3	9	9	1	9	9	8	8	6	7	2
e											4	8	1	9	0	2	2	4	5	4	5	9	2	8	5	4	8	4	8	1	8	8	2	3	7	9	8	5	4	4	1
											1	2	2	2	2	2	2	2	2	1	2	2	2	2	2	2	2	2	2	1	2	1	1	2	1	2	1	1	1	1	0
											.	.	.	.	.	.	.	.	.	.	.	.	.	.	.	.	.	.	.	.	.	.	.	.	.	.	.	.	.	.	.
N											9	2	0	1	0	1	1	1	1	4	3	1	3	0	1	1	2	3	1	9	2	8	8	0	8	0	7	7	5	6	2
d											5	7	5	4	0	4	9	1	4	5	1	3	7	8	8	9	5	7	5	1	1	6	8	3	2	6	2	7	7	7	0
											0	0	0	0	0	0	0	0	0	0	0	0	0	0	0	0	0	0	0	0	0	0	0	0	0	0	0	0	0	0	0
											.	.	.	.	.	.	.	.	.	.	.	.	.	.	.	.	.	.	.	.	.	.	.	.	.	.	.	.	.	.	.
S											6	6	6	6	8	8	8	8	8	6	8	8	8	8	7	8	8	8	8	7	7	7	8	7	7	5	7	6	5	6	0
m											5	9	7	5	7	5	6	1	8	4	7	9	5	4	9	4	0	0	9	0	7	5	4	3	9	3	0	6	9	2	7
											0	0	0	0	0	0	0	0	0	0	0	0	0	0	0	0	0	0	0	0	0	0	0	0	0	0	0	0	0	0	0
											.	.	.	.	.	.	.	.	.	.	.	.	.	.	.	.	.	.	.	.	.	.	.	.	.	.	.	.	.	.	.
E											3	2	3	3	2	3	2	3	3	2	3	2	3	3	2	2	3	3	3	2	3	3	3	2	2	2	2	2	2	2	0
u											2	9	8	5	6	5	9	6	5	9	4	4	4	3	7	4	2	5	4	5	0	5	1	8	7	9	7	7	4	5	3

Gd											1.09
Dy											1.49
Er											0.93
Yb											0.98
Pb											
Dv	0.042	0.042	0.043	0.044	0.045	0.045	0.043	0.047	0.049	0.047	0.037
$\log fO_2$	-0.21	-0.22	-0.34	-0.50	-0.43	-0.47	-0.47	-0.70	-0.77	-0.80	-0.41
Sc/Y ol$_2$	67.7	76.1	85.9	63.9	80.7	78.6	65.7	73.6	75.1	71.3	84.1
Sc/Y melt*Sc	4.214	4.314	4.514	4.614	4.614	4.614	4.714	5.114	5.114	5.615	4.513

Gd	1.02	1.36	1.13	1.17	1.13	1.34	1.13	1.24	1.00	1.24	1.13	1.21	1.30	1.13
Dy	1.32	1.42	1.71	1.35	1.56	1.64	1.66	1.59	0.85	1.79	1.58	1.72	1.22	1.62
Er	0.83	1.02	1.00	0.65	1.07	1.05	1.04	0.94	0.66	1.31	0.85	1.03	0.97	1.02
Yb	0.84	1.00	1.22	0.69	0.84	1.08	1.03	0.97	0.80	0.90	1.03	1.12	1.00	1.18
Pb	0.08	0.20	0.20	0.14	0.22	0.20	0.17	0.10		0.19		0.19	0.20	0.18
Dv	0.037	0.038	0.038	0.036	0.038			0.038	0.038	0.039	0.039	0.039	0.039	0.038
$\log fO_2$	-0.37	-0.30	-0.29	-0.31	-0.40			-0.42	-0.45	-0.43	-0.41	-0.49	-0.45	-0.43
Sc/Y ol$_2$	66.9	92.3	103.7	70.6	66.9			68.4	68.4	79.0	84.6	68.4	85.0	72.4
Sc/Y melt*Sc	4.014	4.113	4.013	4.114	4.114			4.114	4.114	4.213	4.213	4.214	4.213	4.214

Gd	1.15	1.14	1.24	1.39	1.11	1.01	1.05	1.07	1.23	1.15	1.06	0.98	0.98	0.87	0.92	0.11
Dy	1.61	1.63	1.59	1.81	1.46	1.46	1.56	1.07	1.49	1.41	1.23	1.17	1.23	1.09	1.16	0.14
Er	1.05	0.98	1.15	0.91	0.83	0.88	1.03	0.78	0.97	0.78	0.83	0.76	0.79	0.70	0.74	0.09
Yb	1.19	1.06	0.91	1.00	0.98	1.02	0.77	0.83	0.87	0.73	0.69	0.80	0.73	0.65	0.69	0.08
Pb	0.21		0.20	0.17	0.17	0.14	0.12	0.05	0.14	0.16	0.15	0.10	0.11	0.10	0.11	0.01
Dv	0.038	0.038	0.039	0.039	0.040	0.041	0.039	0.038	0.044	0.039	0.040					
$\log fO_2$	-0.45	-0.45	-0.52	-0.50	-0.54	-0.71	-0.61	-0.57	-0.87	-0.69	-0.70	-1.00	-1.10	-1.10	-1.10	0.08
Sc/Y ol$_2$	81.5	80.0	84.3	84.3	87.6	61.5	70.3	73.7	61.0	62.9	62.9					
Sc/Y melt*Sc	4.313	4.313	4.413	4.413	4.513	4.514	4.614	4.614	4.715	4.815	4.815					

	/Y	34	12	00	84	19	29	83	80	76	24	99			22	39	09	10		25			23	25	86	73		30	75	18		94	98		89	89			86		87	57	43	04	03		06												
	TFe/MgT													1388	1388	1388		1392	1396		1391	1397		1400	1398				1409					1421					1425		1429	1432		1437	1439	1444	1446	1446	1449	1449	1440	1486	1540	1513	54
Host olivine	Fo, mol%	91.05	91.33	91.85	91.91	91.91	91.99	92.05	92.67	92.70	93.26	92.02	91.46	90.92	90.92	90.97	91.01	91.16	91.08	91.11	91.12	91.19		91.10	91.22	91.28	91.36	91.40	91.46	91.49	91.50	91.55	91.60	91.65	91.75	91.78	91.87	91.90	91.91	91.94	92.08	92.14	92.20	92.27	92.34	92.45	92.50	92.50	92.81	92.89	92.52	92.05
EPMA, wt.%	Al_2O_3	0.00	0.00	0.00	0.00	0.00	0.00	0.00	0.00	0.00	0.00	0.00		0.00	0.00	0.00	0.00	0.00	0.00	0.00	0.00	0.00		0.00	0.00	0.00	0.00	0.00	0.00	0.00	0.00	0.00	0.00	0.00	0.00	0.00	0.00	0.00	0.00	0.00	0.00	0.00	0.00	0.00	0.00	0.00	0.00	0.00	0.00	0.00	0.00	0.00
	CaO	0.06	0.06	0.05	0.05	0.05	0.06	0.05	0.06	0.06	0.06	0.06		0.07	0.07	0.06	0.06	0.06	0.06	0.06	0.05	0.05	0.06	0.05	0.05	0.06	0.06	0.04	0.05	0.05	0.09	0.05	0.05	0.06	0.06	0.06	0.06	0.06	0.04	0.04	0.06	0.05	0.05	0.07	0.07	0.07	0.07	0.07	0.07	0.07	0.07	0.07
	TiO_2	0.00	0.00	0.00	0.00	0.00	0.00	0.00	0.00	0.00	0.00	0.00		0.00	0.00	0.00	0.00	0.00	0.00	0.00	0.00	0.00	0.06	0.00	0.00	0.00	0.00	0.00	0.00	0.00	0.00	0.00	0.00	0.00	0.00	0.00	0.00	0.00	0.00	0.00	0.00	0.00	0.00	0.00	0.00	0.00	0.00	0.00	0.00	0.00	0.00	0.00
	NiO	0.43	0.44	0.45	0.45	0.45	0.45	0.45	0.46	0.46	0.46	0.45		0.44	0.44	0.44	0.43	0.44	0.44	0.44	0.44	0.44	0.44	0.44	0.45	0.44	0.44	0.45	0.44	0.45	0.45	0.45	0.45	0.46	0.45	0.45	0.45	0.45	0.46	0.46	0.46	0.46	0.46	0.46	0.46	0.46	0.46	0.46	0.46	0.46	0.42	0.45

	MnO	Cr_2O_3	MgO	FeO	SiO_2	Total	Sc	V	Co	Cu	Zn
	3	0	3	0	1	2	5	6	5	6	4
	0	0	0	0	0	0	0	0	0	0	0
	0.135	0.133	0.126	0.125	0.123	0.120	0.115	0.114	0.104	0.124	0.119
	0	0	0	0	0	0	0	0	0	0	0
	2.109	2.104	2.045	2.050	2.055	2.048	1.976	1.976	1.765	2.051	2.049
	0.049	0.049	0.045	0.050	0.050	0.050	0.050	0.050	0.051	0.055	0.054
	6.339	6.937	4.747	3.717	4.748	4.833	3.397	8.585	3.333	49.840	3.777
	8.699	8.454	7.991	9.112	9.242	8.447	7.519	1.949	1.414	8.581	6.611
	40.888	41.029	40.969	41.019	41.085	41.122	40.022	42.219	41.930	40.833	41.903
	1	1	1	1	1	1	1	1	1	1	1
	0	0	0	0	0	9	9	0	0	0	0
	1	0	0	0	0	9	8	0	0	0	0
	0.447	0.445	0.476	0.439	0.459	0.469	0.452	0.439	0.423	100.325	0.444
	4.747	4.763	4.739	4.769	4.755	4.768	4.777	4.783	4.776	4.768	4.776
	4.773	4.772	4.773	4.773	4.773	4.773	4.773	4.773	4.773	4.773	4.773
	3.321	2.272	2.373	4.404	4.013	4.009	0.316	3.669	6.999	4.025	3.324
	6.666	6.666	6.666	6.666	6.666	6.666	6.666	6.666	6.666	6.666	6.666
	5.902	6.666	5.745	5.574	5.427	5.902	5.902	5.902	5.902	5.902	5.902
	2.758	2.758	2.758	2.758	2.758	2.758	2.758	2.758	2.758	2.758	2.758
	1.772	1.772	1.772	1.772	1.772	1.772	1.772	1.772	1.772	1.772	1.772
	2.772	2.772	2.772	2.772	2.772	2.772	2.772	2.772	2.772	2.772	2.772
	3.772	3.772	3.772	3.772	3.772	3.772	3.772	3.772	3.772	3.772	3.772
	4.772	4.772	4.772	4.772	4.772	4.772	4.772	4.772	4.772	4.772	4.772
	5.772	5.772	5.772	5.772	5.772	5.772	5.772	5.772	5.772	5.772	5.772
	6.772	6.772	6.772	6.772	6.772	6.772	6.772	6.772	6.772	6.772	6.772
	7.772	7.772	7.772	7.772	7.772	7.772	7.772	7.772	7.772	7.772	7.772
	8.772	8.772	8.772	8.772	8.772	8.772	8.772	8.772	8.772	8.772	8.772
	9.772	9.772	9.772	9.772	9.772	9.772	9.772	9.772	9.772	9.772	9.772
	10.772	10.772	10.772	10.772	10.772	10.772	10.772	10.772	10.772	10.772	10.772
	11.772	11.772	11.772	11.772	11.772	11.772	11.772	11.772	11.772	11.772	11.772
	12.772	12.772	12.772	12.772	12.772	12.772	12.772	12.772	12.772	12.772	12.772
	13.772	13.772	13.772	13.772	13.772	13.772	13.772	13.772	13.772	13.772	13.772
	14.772	14.772	14.772	14.772	14.772	14.772	14.772	14.772	14.772	14.772	14.772
	15.772	15.772	15.772	15.772	15.772	15.772	15.772	15.772	15.772	15.772	15.772
	16.772	16.772	16.772	16.772	16.772	16.772	16.772	16.772	16.772	16.772	16.772
	17.772	17.772	17.772	17.772	17.772	17.772	17.772	17.772	17.772	17.772	17.772
	18.772	18.772	18.772	18.772	18.772	18.772	18.772	18.772	18.772	18.772	18.772
	19.772	19.772	19.772	19.772	19.772	19.772	19.772	19.772	19.772	19.772	19.772
	20.772	20.772	20.772	20.772	20.772	20.772	20.772	20.772	20.772	20.772	20.772
	21.772	21.772	21.772	21.772	21.772	21.772	21.772	21.772	21.772	21.772	21.772
	22.772	22.772	22.772	22.772	22.772	22.772	22.772	22.772	22.772	22.772	22.772
	23.772	23.772	23.772	23.772	23.772	23.772	23.772	23.772	23.772	23.772	23.772
	24.772	24.772	24.772	24.772	24.772	24.772	24.772	24.772	24.772	24.772	24.772
	25.772	25.772	25.772	25.772	25.772	25.772	25.772	25.772	25.772	25.772	25.772
	26.772	26.772	26.772	26.772	26.772	26.772	26.772	26.772	26.772	26.772	26.772
	27.772	27.772	27.772	27.772	27.772	27.772	27.772	27.772	27.772	27.772	27.772
	28.772	28.772	28.772	28.772	28.772	28.772	28.772	28.772	28.772	28.772	28.772
	29.772	29.772	29.772	29.772	29.772	29.772	29.772	29.772	29.772	29.772	29.772
	30.772	30.772	30.772	30.772	30.772	30.772	30.772	30.772	30.772	30.772	30.772
	31.772	31.772	31.772	31.772	31.772	31.772	31.772	31.772	31.772	31.772	31.772
	32.772	32.772	32.772	32.772	32.772	32.772	32.772	32.772	32.772	32.772	32.772
	33.772	33.772	33.772	33.772	33.772	33.772	33.772	33.772	33.772	33.772	33.772
	34.772	34.772	34.772	34.772	34.772	34.772	34.772	34.772	34.772	34.772	34.772
	35.772	35.772	35.772	35.772	35.772	35.772	35.772	35.772	35.772	35.772	35.772
	36.772	36.772	36.772	36.772	36.772	36.772	36.772	36.772	36.772	36.772	36.772
	37.772	37.772	37.772	37.772	37.772	37.772	37.772	37.772	37.772	37.772	37.772
	38.772	38.772	38.772	38.772	38.772	38.772	38.772	38.772	38.772	38.772	38.772
	39.772	39.772	39.772	39.772	39.772	39.772	39.772	39.772	39.772	39.772	39.772
	40.772	40.772	40.772	40.772	40.772	40.772	40.772	40.772	40.772	40.772	40.772
	41.772	41.772	41.772	41.772	41.772	41.772	41.772	41.772	41.772	41.772	41.772
	42.772	42.772	42.772	42.772	42.772	42.772	42.772	42.772	42.772	42.772	42.772
	43.772	43.772	43.772	43.772	43.772	43.772	43.772	43.772	43.772	43.772	43.772
	44.772	44.772	44.772	44.772	44.772	44.772	44.772	44.772	44.772	44.772	44.772
	45.772	45.772	45.772	45.772	45.772	45.772	45.772	45.772	45.772	45.772	45.772
	46.772	46.772	46.772	46.772	46.772	46.772	46.772	46.772	46.772	46.772	46.772
	47.772	47.772	47.772	47.772	47.772	47.772	47.772	47.772	47.772	47.772	47.772
	48.772	48.772	48.772	48.772	48.772	48.772	48.772	48.772	48.772	48.772	48.772
	49.772	49.772	49.772	49.772	49.772	49.772	49.772	49.772	49.772	49.772	49.772
	50.772	50.772	50.772	50.772	50.772	50.772	50.772	50.772	50.772	50.772	50.772
	51.772	51.772	51.772	51.772	51.772	51.772	51.772	51.772	51.772	51.772	51.772
	52.772	52.772	52.772	52.772	52.772	52.772	52.772	52.772	52.772	52.772	52.772
	53.772	53.772	53.772	53.772	53.772	53.772	53.772	53.772	53.772	53.772	53.772
	54.772	54.772	54.772	54.772	54.772	54.772	54.772	54.772	54.772	54.772	54.772
	55.772	55.772	55.772	55.772	55.772	55.772	55.772	55.772	55.772	55.772	55.772
	56.772	56.772	56.772	56.772	56.772	56.772	56.772	56.772	56.772	56.772	56.772
	57.772	57.772	57.772	57.772	57.772	57.772	57.772	57.772	57.772	57.772	57.772
	58.772	58.772	58.772	58.772	58.772	58.772	58.772	58.772	58.772	58.772	58.772
	59.772	59.772	59.772	59.772	59.772	59.772	59.772	59.772	59.772	59.772	59.772
	60.772	60.772	60.772	60.772	60.772	60.772	60.772	60.772	60.772	60.772	60.772
	61.772	61.772	61.772	61.772	61.772	61.772	61.772	61.772	61.772	61.772	61.772
	62.772	62.772	62.772	62.772	62.772	62.772	62.772	62.772	62.772	62.772	62.772
	63.772	63.772	63.772	63.772	63.772	63.772	63.772	63.772	63.772	63.772	63.772
	64.772	64.772	64.772	64.772	64.772	64.772	64.772	64.772	64.772	64.772	64.772
	65.772	65.772	65.772	65.772	65.772	65.772	65.772	65.772	65.772	65.772	65.772
	66.772	66.772	66.772	66.772	66.772	66.772	66.772	66.772	66.772	66.772	66.772
	67.772	67.772	67.772	67.772	67.772	67.772	67.772	67.772	67.772	67.772	67.772
	68.772	68.772	68.772	68.772	68.772	68.772	68.772	68.772	68.772	68.772	68.772
	69.772	69.772	69.772	69.772	69.772	69.772	69.772	69.772	69.772	69.772	69.772
	70.772	70.772	70.772	70.772	70.772	70.772	70.772	70.772	70.772	70.772	70.772
	71.772	71.772	71.772	71.772	71.772	71.772	71.772	71.772	71.772	71.772	71.772
	72.772	72.772	72.772	72.772	72.772	72.772	72.772	72.772	72.772	72.772	72.772
	73.772	73.772	73.772	73.772	73.772	73.772	73.772	73.772	73.772	73.772	73.772
	74.772	74.772	74.772	74.772	74.772	74.772	74.772	74.772	74.772	74.772	74.772
	75.772	75.772	75.772	75.772	75.772	75.772	75.772	75.772	75.772	75.772	75.772
	76.772	76.772	76.772	76.772	76.772	76.772	76.772	76.772	76.772	76.772	76.772
	77.772	77.772	77.772	77.772	77.772	77.772	77.772	77.772	77.772	77.772	77.772
	78.772	78.772	78.772	78.772	78.772	78.772	78.772	78.772	78.772	78.772	78.772
	79.772	79.772	79.772	79.772	79.772	79.772	79.772	79.772	79.772	79.772	79.772
	80.772	80.772	80.772	80.772	80.772	80.772	80.772	80.772	80.772	80.772	80.772
	81.772	81.772	81.772	81.772	81.772	81.772	81.772	81.772	81.772	81.772	81.772
	82.772	82.772	82.772	82.772	82.772	82.772	82.772	82.772	82.772	82.772	82.772
	83.772	83.772	83.772	83.772	83.772	83.772	83.772	83.772	83.772	83.772	83.772
	84.772	84.772	84.772	84.772	84.772	84.772	84.772	84.772	84.772	84.772	84.772
	85.772	85.772	85.772	85.772	85.772	85.772	85.772	85.772	85.772	85.772	85.772
	86.772	86.772	86.772	86.772	86.772	86.772	86.772	86.772	86.772	86.772	86.772
	87.772	87.772	87.772	87.772	87.772	87.772	87.772	87.772	87.772	87.772	87.772
	88.772	88.772	88.772	88.772	88.772	88.772	88.772	88.772	88.772	88.772	88.772
	89.772	89.772	89.772	89.772	89.772	89.772	89.772	89.772	89.772	89.772	89.772
	90.772	90.772	90.772	90.772	90.772	90.772	90.772	90.772	90.772	90.772	90.772
	91.772	91.772	91.772	91.772	91.772	91.772	91.772	91.772	91.772	91.772	91.772
	92.772	92.772	92.772	92.772	92.772	92.772	92.772	92.772	92.772	92.772	92.772
	93.772	93.772	93.772	93.772	93.772	93.772	93.772	93.772	93.772	93.772	93.772
	94.772	94.772	94.772	94.772	94.772	94.772	94.772	94.772	94.772	94.772	94.772
	95.772	95.772	95.772	95.772	95.772	95.772	95.772	95.772	95.772	95.772	95.772
	96.772	96.772	96.772	96.772	96.772	96.772	96.772	96.772	96.772	96.772	96.772
	97.772	97.772	97.772	97.772	97.772	97.772	97.772	97.772	97.772	97.772	97.772
	98.772	98.772	98.772	98.772	98.772	98.772	98.772	98.772	98.772	98.772	98.772
	99.772	99.772	99.772	99.772	99.772	99.772	99.772	99.772	99.772	99.772	99.772
	100.772	100.772	100.772	100.772	100.772	100.772	100.772	100.772	100.772	100.772	100.772

LA-ICP-MS, ppm

n											9	5	7	5	5	5	3	3	2	5	3	3	4	1	2	9	9	1	7	8	2	8	0	1	1	1
											.	.	.	.	.	.	.	.	.	.	.	.	.	.	.	.	.	.	.	.	.	.	.	.	.	.
											1	9	0	5	0	9	4	4	5	1	4	6	5	1	9	1	1	1	8	9	3	1	1	0	0	0
	0	0	0	0	0	0	0	0	0	0	0	0	0	0	0	0	0	0	0	0	0	0	0	0	0	0	0	0	0	0	0	0	0	0	0	0
	.	.	.	.	.	.	.	.	.	.	.	.	.	.	.	.	.	.	.	.	.	.	.	.	.	.	.	.	.	.	.	.	.	.	.	.
	0	0	0	0	0	0	0	0	0	0	0	0	0	0	0	0	0	0	0	0	0	0	0	0	0	0	0	0	0	0	0	0	0	0	0	0
Y	6	6	5	7	6	5	6	5	6	5	4	7	4	4	6	7	6	6	5	5	6	4	5	5	5	5	5	4	7	7	6	5	7	6	6	6

*Mz-4 series melt compositions were calculated as a function of Fo contents of the measured olivine. Major element contents of the olivine by Sobolev et al., 2007.

[1]Z6-Cl- extremely Cl rich melt inclusion

[2]Sc/Y* melt is calculated as a function of MgO - see Methods) and host olivine major and trace element compositions.